MDPI

Article

OpenSeismoMatlab: New Features, Verification and Charting Future Endeavors

George Papazafeiropoulos [1] and Vagelis Plevris [2,*]

[1] School of Civil Engineering, National Technical University of Athens, 15772 Athens, Greece; gpapazafeiropoulos@yahoo.gr

[2] Department of Civil and Environmental Engineering, Qatar University, Doha P.O. Box 2713, Qatar

* Correspondence: vplevris@qu.edu.qa

Abstract: To facilitate the precise design of earthquake-resistant structures, it is imperative to accurately evaluate the impact of seismic events on these constructions and predict their responses. OpenSeismoMatlab, a robust, free ground motion data processing software, plays a pivotal role in this endeavor. It empowers users to compute a wide array of outcomes using input acceleration time histories, encompassing time histories themselves, as well as linear and nonlinear spectra. These capabilities are instrumental in supporting structural design initiatives. This study provides a comprehensive exposition of the latest version (v 5.05) of OpenSeismoMatlab. It delves into intricate facets of the software, encompassing a detailed exploration of the input and output variables integral to each operational category. Comprehensive calculation flowcharts are presented to elucidate the software's organizational structure and operational sequences. Furthermore, a meticulous verification assessment is conducted to validate OpenSeismoMatlab's performance. This verification entails a rigorous examination of specific cases drawn from existing literature, wherein the software's outcomes are rigorously compared against corresponding results from prior studies. The examination not only underscores the reliability of OpenSeismoMatlab but also emphasizes its ability to generate outcomes that closely align with findings documented in the established body of literature. Concluding the study, the paper outlines potential directions for future research, shedding light on avenues where further development and exploration can enhance the utility and scope of OpenSeismoMatlab in advancing seismic engineering and structural design practices.

Keywords: OpenSeismoMatlab; earthquake; seismic design; nonlinear spectra; pulse; resampling

1. Introduction

The seismic-induced dynamic response of buildings is a critical factor in determining the extent of damage and casualties arising from earthquake events. Accurately predicting this response beforehand is a complex task, largely owing to the unpredictable and random characteristics of seismic forces. Strong ground motion analysis software assumes a pivotal role in both qualitative and quantitative assessments of seismic impacts on buildings. These software tools possess the capability to scrutinize intricate characteristics of input ground motion and facilitate estimations concerning the response and potential damage sustained by structures when subjected to seismic excitation. Furthermore, strong motion processing software can contribute to the validation and refinement of various seismic code provisions, thereby enhancing structural design practices and reducing vulnerability to seismic risks. Moreover, these software applications offer a substantial advantage by affording insights into the intricate interplay between seismic events and structures, thereby enabling designers to ensure the safety of building occupants and the overall capacity of the structure to withstand future seismic events.

In this study, we introduce, describe, and validate the new version of the OpenSeismoMatlab software suite for strong ground motion processing, aimed at facilitating the

assessment of seismic effects on structures. An earlier open-source version of this software was presented in [1], comprehensively elucidating its structure, algorithms, and core routines. Additionally, the article featured detailed results comparing various spectral aspects of 11 earthquake-induced strong ground motions with those obtained using proprietary software. Since then, significant strides have been made to enhance the software's performance, refine its accuracy, and streamline its architecture to facilitate future extensions. The present work serves a three-fold purpose:

1. Elaborate on the new capabilities of OpenSeismoMatlab, including a comprehensive presentation of input/output variables for its various routines and, when necessary, flowcharts depicting the calculation process (Section 2 of this study).
2. Demonstrate OpenSeismoMatlab's capacity to yield highly accurate and reliable results. To achieve this, we replicated several cases from existing literature using OpenSeismoMatlab and compared the outcomes with those obtained through alternative methods (Section 3 of this study).
3. Offer insights into prospective avenues for further research in two dimensions: (i) the refinement of OpenSeismoMatlab itself, and (ii) the advancement of seismic building design methodologies, leveraging OpenSeismoMatlab as a foundational tool (Section 4 of this study).

The updated version of OpenSeismoMatlab, as showcased in this study and compared to its earlier version outlined in [1] marks a significant enhancement in seismic analysis capabilities. This version incorporates numerous novel features, enhancing the user's ability to conduct thorough evaluations of earthquake data and extract an expanded array of seismic parameters. Key updates include high-pass and low-pass filtering options for ground motion frequency content, and resampling functionalities, allowing for more precise customization of earthquake time histories to meet specific needs. The addition of rigid-plastic sliding response spectra and constant strength response spectra offers a refined perspective on seismic reactions under diverse conditions. The new pulse decomposition feature enables detailed seismic signal analysis, facilitating a more in-depth examination of ground motion traits. Furthermore, this latest version supports incremental dynamic analysis, aiding in the systematic evaluation of structural responses to varying seismic intensities. These enhancements collectively boost the software's utility, equipping researchers and engineers with a comprehensive toolkit for the detailed characterization and analysis of earthquake phenomena. Notably, this version has been employed for various estimations and assessments of building responses to earthquakes, such as in the studies of the 6 February 2023, Kahramanmaras earthquake in Turkey (refer to [2]), and its core analytical methods have been applied in seismic building design elsewhere [3].

2. Structure and New Functionalities of OpenSeismoMatlab

The OpenSeismoMatlab software accepts three standard input parameters in a specific order: first, the time step of the input acceleration time history (or signal); second, the acceleration time history itself; and third, a user-defined switch that specifies the desired processing mode for the input time history. This final parameter, presented as a string input, also dictates the additional input variables required by OpenSeismoMatlab to successfully process the input signal. Table 1 provides an overview of the various acceptable syntaxes for the OpenSeismoMatlab function. Notably, the syntaxes present in the initial version of OpenSeismoMatlab, as described in [1], retain this reference citation.

The newly introduced functionalities of OpenSeismoMatlab in its current version are elucidated herein.

Table 1. Acceptable syntaxes of the OpenSeismoMatlab function and corresponding processing tasks or output of each option.

Syntax	Task
PARAM = OpenSeismoMatlab(DT,XGTT,SW,__)	General syntax with default input (switch is needed)
PARAM = OpenSeismoMatlab(DT,XGTT,'ARIAS')	Arias intensity, cumulative energy, significant duration [1]
PARAM = OpenSeismoMatlab(DT,XGTT,. . . 'BUTTERWORTHHIGH',BORDER,FLC)	High-pass Butterworth filter
PARAM = OpenSeismoMatlab(DT,XGTT,. . . 'BUTTERWORTHLOW',BORDER,FHC)	Low-pass Butterworth filter
PARAM = OpenSeismoMatlab(DT,XGTT,'CDRS',T,KSI,MU,PYSF,DTTOL,ALGID, RINF,MAXTOL,JMAX,DAK)	Constant ductility response spectrum [1]
PARAM = OpenSeismoMatlab (DT,XGTT,'CSRS',T,KSI,FYR,PYSF,DTTOL,ALGID, RINF,MAXTOL,JMAX,DAK)	Constant strength response spectrum
PARAM = OpenSeismoMatlab (DT,XGTT,'ELRS',T,KSI,ALGID,RINF,DTTOL)	Linear elastic response spectrum [1]
PARAM = OpenSeismoMatlab(DT,XGTT,'EPGA')	Effective peak ground acceleration
PARAM = OpenSeismoMatlab(DT,XGTT,'FAS')	Fourier amplitude spectrum [1]
PARAM = OpenSeismoMatlab(DT,XGTT,'IDA',T,. . . LAMBDAF,IM_DM,M,UY,PYSF,KSI,ALGID,U0,UT0,. . . RINF,MAXTOL,JMAX,DAK)	Incremental dynamic analysis of SDOF system
PARAM = OpenSeismoMatlab(DT,XGTT,'PGA')	Peak ground acceleration [1]
PARAM = OpenSeismoMatlab(DT,XGTT,'PGD')	Peak ground displacement [1]
PARAM = OpenSeismoMatlab(DT,XGTT,'PGV')	Peak ground velocity [1]
PARAM = OpenSeismoMatlab (DT,XGT,'PULSEDECOMP',WNAME,TPMIN, TPMAX,NSCALES)	Pulse decomposition
PARAM = OpenSeismoMatlab(DT,XGTT, 'SINCRESAMPLE',DTI)	Resampling (change time step size)
PARAM = OpenSeismoMatlab(DT,XGTT,'RPSRS',CF,. . . ALGID,RINF,MAXTOL,JMAX,DAK)	Rigid-plastic sliding response spectrum
PARAM = OpenSeismoMatlab(DT,XGTT,'SIH1952')	Spectral intensity [4]
PARAM = OpenSeismoMatlab(DT,XGTT,'SINH1984')	Spectral intensity [5]
PARAM = OpenSeismoMatlab(DT,XGTT,'TIMEHIST',. . . BASELINESW)	Velocity and displacement time histories with baseline correction or not [1]

2.1. High-Pass and Low-Pass Butterworth Filter

Initially, the design of a high-pass or low-pass Butterworth filter is conducted, contingent upon the user's label specification ('BUTTERWORTHHIGH' and 'BUTTERWORTHLOW,' respectively). The transfer function for the nth order digital Butterworth filter, as employed within OpenSeismoMatlab, is expressed as follows:

$$H(z) = \frac{b(1) + b(2)z^{-1} + \ldots + b(n+1)z^{-n}}{a(1) + a(2)z^{-1} + \ldots + a(n+1)z^{-n}} \tag{1}$$

where the vectors b and a encompass the transfer function coefficients pertinent to the Butterworth filter. Following the aforementioned Butterworth filter design, a zero-phase digital filtering operation is executed, involving the processing of the input time history in both forward and reverse directions, thereby achieving zero-phase distortion. Detailed insights into the filtering algorithm can be found in [6]. For clarity, Table 2 in this manuscript provides an inventory of notations, default values, and explanations of input and output parameters within OpenSeismoMatlab, specifically for high-pass and low-pass filtering of ground motions ('BUTTERWORTHHIGH' and 'BUTTERWORTHLOW,' respectively).

Table 2. Notation, default values, and description of input and output arguments of OpenSeismo-Matlab for high- and low-pass filtering of ground motions.

Notation	Default	Description
Input		
DT	(-) s	Time step of the input acceleration time history XGTT
XGTT	(-) m/s^2	Input acceleration time history
BORDER	4	Order of Butterworth filter
FLC	0.1 Hz	Low cutoff frequency (for 'BUTTERWORTHHIGH')
FHC	10 Hz	High cutoff frequency (for 'BUTTERWORTHLOW')
Output		
ACC	-	Filtered acceleration

The filtering of ground motion data serves several essential purposes. High-pass filtering, alternatively referred to as low-cut filtering, facilitates stable double-integration, thereby enabling the derivation of a reliable ground displacement time history [7]. It is noteworthy that baseline correction, a widely employed technique for computing ground displacement from ground acceleration time histories, is among the capabilities offered by OpenSeismoMatlab. Baseline correction essentially represents a rudimentary form of high-pass filtering applied to raw ground motion data. Consequently, the ground motion filtering capability within OpenSeismoMatlab extends beyond baseline correction, affording enhanced precision in calculations.

Conversely, low-pass filtering is instrumental in mitigating the high-frequency components introduced using seismometer instruments, which can introduce noise into the acceleration time history. Both low-pass and high-pass filtering processes exert a profound influence on building design. The frequency content of the ground motion employed for dynamic analysis of a building plays a pivotal role in determining whether resonance occurs, potentially leading to a heightened dynamic response. Furthermore, the choice of dynamic time integration algorithms for analysis hinges upon the frequency characteristics, as it affects the accuracy of the building's response calculations.

In addition to the considerations outlined above, the filtering of ground motion time histories, particularly high-pass filtering, demands meticulous attention, as it may potentially interfere with critical ground motion components, such as the fling-step effect [8]. As an illustrative instance, the Chi-Chi earthquake of 1999 featured fling components with an approximate frequency of 0.07 Hz, a characteristic readily addressed with a low-cut filter [9]. The removal of these effects can exert a significant influence on the computed seismic response, notably for spatially extensive engineering structures traversing fault rupture zones.

For building structures of up to 30 stories, the natural frequencies at a fixed base typically range from 0.4 Hz to 15 Hz. The lower limit can further decrease to 0.2 Hz when inelasticity and soil-structure interaction phenomena are taken into account. Consequently, the selection of frequency limits for filtering necessitates careful consideration to encompass the aforementioned frequency range. Moreover, it is evident that the filtering process can wield a substantial impact on response spectra, which serve as fundamental tools for the design of buildings and other engineering structures [10]. The integration of filtering capabilities into the latest version of OpenSeismoMatlab emerges as a critical functionality for earthquake engineering practitioners. Future developments will extend the repertoire of advanced filtering techniques within OpenSeismoMatlab.

2.2. Constant Ductility and Constant Strength Response Spectra (CDRS and CSRS)

Constant strength response spectra and constant ductility response spectra serve as foundational elements in shaping the design spectra for building structures in numerous seismic codes adopted globally. The core principle underpinning the concept of inelastic structural design involves the establishment of a reduction factor. This factor is applied to a fundamental elastic (pseudo)acceleration spectrum, primarily to accommodate desired

levels of ductility and overstrength [11]. The resultant reduced acceleration spectrum is subsequently employed in the elastic design of the structure. The determination of these reduction factors encompasses various methodologies, including an examination of the relationship between inelastic and elastic response spectra, empirical investigations, and the expertise and judgment of building code authorities and developers [12].

Both types of inelastic spectra, namely the constant ductility response spectra and the constant strength response spectra, have been incorporated into the most recent iteration of OpenSeismoMatlab. Corresponding switches for activating these two spectrum types are denoted as 'CDRS' and 'CSRS,' respectively. The former category was previously introduced in the initial release of OpenSeismoMatlab. However, in the latest version expounded upon in this study, significant enhancements have been made, primarily focusing on computational efficiency. As such, it is reintroduced and discussed in detail within this investigation. Furthermore, the latest software release introduces the constant strength response spectrum as a new addition.

The constant ductility response spectra provide essential information, including the maximum inelastic response, utilizing the elastic bilinear model with kinematic hardening implemented in OpenSeismoMatlab. These spectra also establish the requisite yield strength for a single-degree-of-freedom (SDOF) system with a given small strain eigenperiod, damping ratio, and post-yield stiffness factor (i.e., the ratio of post-yield stiffness to small strain stiffness) to attain a predefined level of displacement ductility (i.e., the ratio of maximum displacement to yield displacement). In cases where multiple strength values correspond to the target displacement ductility, the highest strength value is retained for consideration. For clarity, Table 3 in this study provides a comprehensive overview of notations, default values, and explanations of input and output parameters indispensable for OpenSeismoMatlab to perform calculations related to the constant ductility response spectrum.

Table 3. Notation, default values, and description of input and output arguments of OpenSeismoMatlab for constant ductility response spectra ('CDRS').

Notation	Default	Description
Input		
DT	(-) s	Time step of the input acceleration time history XGTT
XGTT	(-) m/s^2	Input acceleration time history
T	[0.02, 50] s	Eigenperiods for which the response spectra are requested
KSI	0.05	Fraction of critical viscous damping
MU	2	Target ductility
N	100	Maximum number of convergence iterations
PYSF	0.01	Post-yield stiffness factor (ratio of post-yield stiffness to small strain stiffness)
DTTOL	0.01	Tolerance for resampling of XGTT
Output		
PSA	-	Pseudoacceleration
PSV	-	Pseudovelocity
SD	-	Spectral displacement
SV	-	Spectral velocity
SA	-	Spectral acceleration
FYK	-	Yield strength corresponding to target ductility MU
MUK	-	Ductility achieved. Must be close to MU
ITERK	-	Iterations needed for convergence to MUK

Figure 1 presents a flowchart delineating the computational sequence, elucidating the sequential execution of program steps within OpenSeismoMatlab for the generation of the constant ductility response spectrum. Noteworthy features of this enhanced algorithm include a preliminary assessment of the time step size for each eigenperiod value before initiating the dynamic response calculations for the respective single-degree-of-freedom (SDOF) oscillator. This pre-check ensures the attainment of sufficiently accurate time

integration results. Furthermore, the algorithm refines the initial bounding yield strength limits that serve as starting points for the convergence process, employing a judiciously chosen hyperbolic curve. This optimization accelerates the convergence rate, enhancing the efficiency of the algorithm.


```
Input:
    DT,XGTT,T,KSI,MU,PYSF,DTTOL,N

Scan all values of SDOF eigenperiods
    for j=1:length(T)

        Check if DT/T>DTTOL. If yes, then resample XGTT with half time step

        Calculate the dynamic response of the linear SDOF

        Assume maximum yield strength coefficient and calculate minimum
        ductility demand MUMIN

        Assume minimum yield strength coefficient and calculate maximum
        ductility demand MUMAX

        Define a hyperbola based on MUMIN and MUMAX

        Determine yield strengths UY1 and UY2 corresponding to 1.2*mu and
        0.8*mu according to the hyperbola

Convergence iterations
        for k=1:N

            Dynamic analysis for strength UY1, UY2 and calculation of
            corresponding ductility factors MU1, MU2 respectively

            Update UY1 and UY2 based on the relation between MU and MU1, MU2

            Check if UY1-UY2 or MU1-MU2 are below tolerance
Output:
    PSA,PSV,SD,SV,SA,FYK,MUK,ITERK
```

Figure 1. Flowchart for the generation of the constant ductility response spectrum.

The constant strength response spectra provide critical information, including the maximum inelastic response and the displacement ductility requirement, for a single-degree-of-freedom (SDOF) system characterized by specific parameters, namely the small strain eigenperiod, damping ratio, yield strength ratio (i.e., the ratio of yield shear to structure weight), and post-yield stiffness factor. For reference, Table 4 presents a comprehensive compilation of notations, default values, and explanatory details pertaining to the input and output parameters required by OpenSeismoMatlab for the computation of the constant strength response spectrum.

Table 4. Notation, default values, and description of input and output arguments of OpenSeismo-Matlab for constant strength response spectra ('CSRS').

Notation	Default	Description
Input		
DT	(-) s	Time step of the input acceleration time history XGTT
XGTT	(-) m/s^2	Input acceleration time history
T	[0.02, 50] s	Eigenperiods for which the response spectra are requested
KSI	0.05	Fraction of critical viscous damping
FYR	0.1	Yield strength ratio (yield shear to structure weight ratio)
PYSF	0.01	Post-yield stiffness factor (ratio of post-yield stiffness to small strain stiffness)
DTTOL	0.01	Tolerance for resampling of XGTT
Output		
SMU	-	Spectral ductility demand
SD	-	Spectral displacement
SV	-	Spectral velocity
SA	-	Spectral acceleration
SEY	-	Spectral yield energy
SED	-	Spectral damping energy

Figure 2 depicts a flowchart elucidating the calculation procedure for generating the constant strength response spectrum. It is evident that the constant strength response spectrum exhibits a relatively simpler structure when compared to its constant ductility counterpart. This characteristic has previously been underscored in the literature, with a focus on the more intuitive parameters entailed in computing the constant strength response spectrum [12]. Moreover, it has been observed that multiple strength values may correspond to identical target ductility levels, as discussed in previous studies [13].

Input:

`DT,XGTT,T,KSI,FYR,PYSF,DTTOL`

Scan all values of SDOF eigenperiods

`for j=1:length(T)`

Check if DT/T>DTTOL. If yes, then resample XGTT with half time step

Calculate the dynamic response of the nonlinear SDOF

Output:

`SMU,SD,SV,SA,SEY,SED`

Figure 2. Flowchart for the generation of the constant strength response spectrum.

2.3. Effective Peak Ground Acceleration (EPGA)

In situations where an abrupt acceleration peak occurs in the time history, but the overall energy of the ground motion remains relatively low, the peak ground acceleration (PGA) may not adequately reflect the earthquake's damage potential. To address this limitation, alternative earthquake intensity measures have been devised, taking into account both the temporal and frequency characteristics of ground motion records. One such measure is the effective peak ground acceleration (EPGA), which is calculated as the average of spectral acceleration values (using a 5 percent damping spectrum) within the time interval of 0.1 s to 0.5 s. at intervals of 0.02 s., divided by a standard spectral amplification factor of 2.5 [14]. EPGA has demonstrated a strong correlation with structural response and the potential for earthquake-induced damage [15,16]. To compute the EPGA using OpenSeismoMatlab, the appropriate switch is denoted as 'EPGA'.

2.4. Incremental Dynamic Analysis of SDOF System

OpenSeismoMatlab incorporates the capability to conduct incremental dynamic analysis (IDA) [17] on a single-degree-of-freedom (SDOF) system subjected to earthquake excitation provided by the user as input. This analysis focuses on the dynamic response of an SDOF system characterized by a fixed eigenperiod, damping ratio, yield displacement, and post-yield stiffness ratio. The aim is to derive intensity measure (IM)–damage measure (DM) curves. The procedure involves the scaling of the acceleration time history by varying factors. For each scaled motion, a dynamic analysis of the SDOF oscillator is performed, resulting in scalar values for DM and IM. Repeating this process for all scaling factors generates a set of DM and corresponding IM values. The IDA curve, calculated by OpenSeismoMatlab, is essentially a plot of DM values against IM values. Users have the flexibility to select the IM–DM pair as an input argument, with a range of options available through the following switches:

- 'SA_MU': Spectral acceleration–displacement ductility
- 'PGD_MU': Peak displacement–displacement ductility
- 'PGV_MU': Peak velocity–displacement ductility
- 'PGA_MU': Peak acceleration–displacement ductility
- 'SA_DISP': Spectral acceleration–displacement
- 'PGD_DISP': Peak displacement–displacement
- 'PGV_DISP': Peak velocity–displacement
- 'PGA_DISP': Peak acceleration–displacement
- 'SA_VEL': Spectral acceleration–velocity
- 'PGD_VEL': Peak displacement–velocity
- 'PGV_VEL': Peak velocity–velocity
- 'PGA_VEL': Peak acceleration–velocity
- 'SA_ACC': Spectral acceleration–acceleration
- 'PGD_ACC': Peak displacement–acceleration
- 'PGV_ACC': Peak velocity–acceleration
- 'PGA_ACC': Peak acceleration–acceleration

Regarding the remaining input arguments and output parameters relevant to Open-SeismoMatlab's IDA functionality, these are comprehensively presented in Table 5.

Table 5. Notation, default values, and description of input and output arguments of OpenSeismo-Matlab for incremental dynamic analysis ('IDA').

Notation	Default	Description
Input		
DT	(-) s	Time step of the input acceleration time history XGTT
XGTT	(-) m/s^2	Input acceleration time history
T	1 s	Eigenperiod of the SDOF system
LAMBDAF	[0.05, 4]	Scaling factor (λ factor) for the IDA
IM_DM	'SA_DISP'	Intensity Measure (IM)–Damage Measure (DM) pair
M	1 kg	Mass of the SDOF oscillator
UY	0.01 m	Yield displacement
PYSF	0.01	Post-yield stiffness factor (ratio of post-yield stiffness to small strain stiffness)
KSI	0.05	Fraction of critical viscous damping
Output		
DM	-	Values of damage measure
IM	-	Values of intensity measure

Figure 3 shows the flowchart illustrating the calculation flow for the generation of the IDA curve.


```
Input:

    DT,XGTT,T,LAMBDAF,IM-DM,M,UY,PYSF,KSI


    k=length(LAMBDAF);

    for j=1:k


        Calculate Intensity Measure (IM) of scaled motion using
        OpenSeismoMatlab with appropriate switch


        Perform nonlinear dynamic analysis of SDOF


        From dynamic response calculate Damage Measure (DM)

Output:

    DM,IM
```
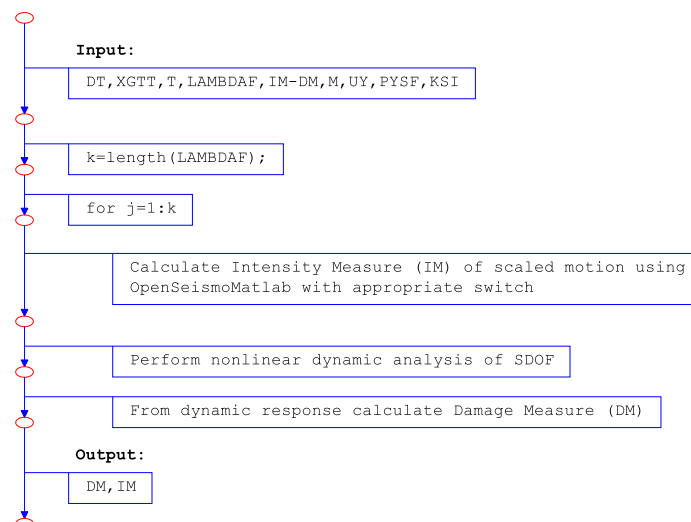
Figure 3. Flowchart for the generation of the incremental dynamic analysis curve.

2.5. Pulse Decomposition

Ground motion time histories recorded in proximity to seismic faults exhibit distinctive characteristics that can heighten the risk of earthquake-induced structural collapse compared to sites located at a greater distance from the fault (far-field sites). A prominent feature of these motions is the presence of a substantial velocity pulse at the outset of the time history, as illustrated in Figure 4 for the 1994 Northridge earthquake (Rinaldi recording).
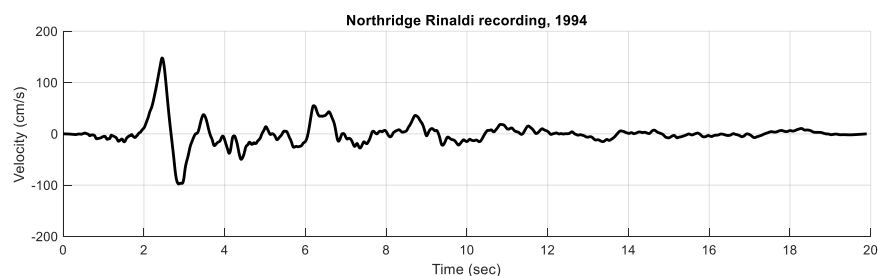
Figure 4. Ground motion record from the 1994 Northridge earthquake (Rinaldi recording), exhibiting a large amplitude pulse early in the velocity time history.

Pulse-like ground motions, exemplified in Figure 4, may arise in near-fault regions when fault rupture progresses towards the site, and the rupture velocity closely approximates the shear wave velocity. This phenomenon results in constructive interference of the wavefront, leading to the arrival of seismic energy from the rupture in the form of a high-amplitude pulse [18,19]. Several key characteristics of pulse-like motions are noted as follows [19]:

- Near-fault pulse-like records tend to induce increased displacement responses, thereby elevating the potential for structural and/or nonstructural damage in both elastic and inelastic structures compared to non-pulse-like motions. Additionally, they tend to produce higher spectral accelerations at longer periods.
- The structural response is significantly influenced by the ratio of the pulse period in the ground motion velocity time history (T_p) to the first-mode period of the building (T_1). When T_p is approximately equal to T_1, elastic structures experience the highest response. In the case of ductile structures, it is presumed that the building's effective fundamental period elongates as damage accumulates. It has been proposed that T_p being approximately twice T_1 may be the most detrimental scenario for structures operating within the nonlinear range. For instances where $T_p < T_1$, such as in tall buildings, the pulse may excite higher modes, leading to substantial displacement and shear force demands in the upper stories.

In light of the aforementioned considerations, it becomes apparent that the ability to discern whether a ground motion exhibits pulse-like characteristics is of paramount significance. A comparative analysis between the original ground motion and the residual signal obtained after subtracting the contained pulse can serve as a means to ascertain the presence of a pulse-like ground motion. OpenSeismoMatlab is equipped with the capability to conduct what is termed a 'pulse decomposition procedure' on any given ground motion time history.

In this pulse decomposition procedure, a continuous wavelet transform is employed to isolate the predominant pulse within the original ground motion, thus facilitating the determination of its significance within the signal [20]. The largest pulse is assumed to align with a predefined standard wavelet type specified by the user and is further scaled by a user-defined factor. The results of this procedure encompass both the extracted pulse and the residual motion, representing the original motion following pulse extraction. Additionally, OpenSeismoMatlab provides information on the pulse period and the scaling factor for the standard wavelet type. The initiation of the pulse decomposition procedure in OpenSeismoMatlab is achieved through the activation of the 'PULSEDECOMP' switch.

For reference, Table 6 offers a comprehensive compilation of input and output parameters relevant to OpenSeismoMatlab's 'PULSEDECOMP' functionality.

Table 6. Notation, default values, and description of input and output arguments of OpenSeismo-Matlab for pulse decomposition analysis.

Notation	Default	Description
Input		
DT	(-) s	Time step of the input acceleration or velocity time history XGTT or XGT
XGTT	(-) m/s^2	Input acceleration time history
XGT	(-) m/s	Input velocity time history
WNAME	Daubechies wavelet of order 4	Wavelet family
TPMIN	0.25 s	Minimum pulse period for continuous wavelet transform
TPMAX	15 s	Maximum pulse period for continuous wavelet transform
NSCALES	50	Number of values between TPMIN and TPMAX
Output		
PULSETH	-	Time history of the pulse
RESTH	-	Time history of the residual motion
TP	-	Period of the extracted pulse
WAVSCALE	-	Scale of largest wavelet found
WAVCOEFS	-	Coefficient for the extracted wavelet

Figure 5 presents a flowchart delineating the computational sequence for the pulse decomposition analysis.
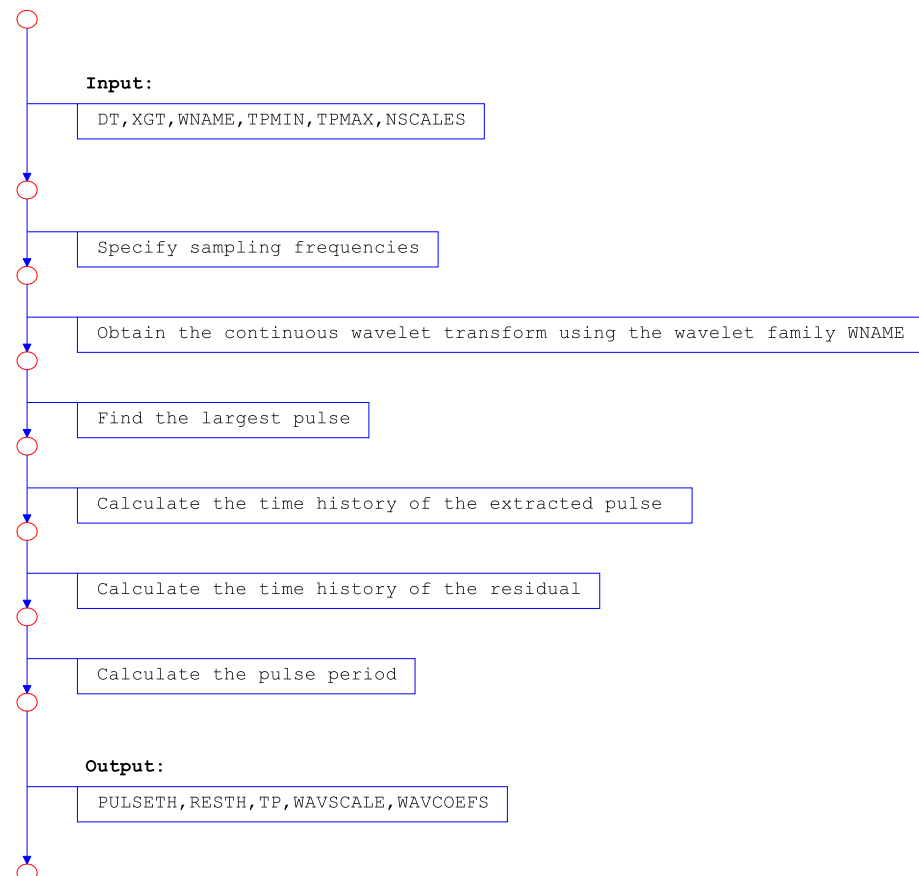
Figure 5. Flowchart for the pulse decomposition analysis.

2.6. Resampling

To mitigate the computational burden associated with the processing of strong ground motion records, several techniques have been proposed to increase the time step of the digitized acceleration time history [21]. Linear interpolation has been employed as a method to reduce the number of time steps required for time integration in the equations of motion when computing response spectra [22]. However, when it comes to resampling digital acceleration time series, sinc interpolation is preferable over the conventional linear interpolation. Sinc interpolation yields superior estimates of peak motions, accurately reproduces acceleration waveforms, avoids underestimating motion near the anti-aliasing corner frequency, and does not introduce spurious energy at high frequencies [23]. Sinc interpolation aligns with the interpolation function that enables the exact recovery of a signal from its sampled values in accordance with the sampling theorem [24].

While linear interpolation offers perfect local interpolation, it falls short in providing smooth interpolation of signals. On the other hand, polynomial interpolation, which ensures perfect smoothness in interpolated signals, is only effective for finite time durations. Sinc interpolation, as demonstrated, strikes a balance between these two extremes, offering maximal smoothness for infinite discrete-time signals. The sinc interpolation function is defined by Formula (2):

$$g(t) = \frac{sin(2\pi F_{max} t)}{2\pi F_{max} t} \tag{2}$$

where F_{max} is the highest frequency contained in the time history. The resampled (interpolated) time history can be expressed as shown in Equation (3):

$$xgtt(t) = \sum_{n=-\infty}^{+\infty} xgtt\left(\frac{n}{F_s}\right) g\left(t - \frac{n}{F_s}\right) \tag{3}$$

where $xgtt\left(\frac{n}{F_s}\right)$ are the samples of $xgtt(t)$ and F_s is the sampling rate, which should be higher than $2F_{max}$ (Nyquist rate). For further insights into this topic, readers are directed to reference [24].

The process of downsampling, which involves reducing the sampling rate of time-series data, imposes constraints on the upper limit for Fourier spectra calculation due to a decrease in the Nyquist frequency. Consequently, this presents limitations for subsequent data utilization. Additionally, downsampling often results in the omission of the highest peak values [25]. It has also been demonstrated that some errors may arise when computing response spectra from decimated (downsampled) motions [23,26].

OpenSeismoMatlab offers the capability to apply sinc resampling to any input time history, activated by specifying the 'SINCRESAMPLE' switch. Table 7 provides a comprehensive overview of the input and output parameters relevant to OpenSeismoMatlab's 'SINCRESAMPLE' functionality. During the resampling process, SINCRESAMPLE assumes that values of the input time history beyond its final time instance are zero. Consequently, significant deviations from zero at the endpoints of the input time history may introduce inaccuracies in the resampled time history at its endpoints.

Table 7. Notation, default values, and description of input and output arguments of OpenSeismoMatlab for sinc resampling.

Notation	Default	Description
Input		
DT	(-) s	Time step of the input acceleration or velocity time history XGTT or XGT
XGTT	(-) m/s^2	Input acceleration time history
DTI	0.01 s	Time step of the resampled time history
Output		
ACC	-	Resampled acceleration time history
TIME	-	Time steps for the resampled acceleration time history

Figure 6 shows the flowchart illustrating the calculation flow for the sinc resampling procedure of an arbitrary input time history.

```
Input:
    DT,XGTT,DTI

    Approximate DT/DTI as a rational fraction M/K

    Append zeros to XGTT such that its length is a multiple of K

    Upsample XGTT by a factor M (time step DT/M)

    Downsample XGTT by a factor K (time step DT*(K/M))

    Truncate padded zeros from the end of the resampled motion so that
    its duration is equal to that of XGTT

Output:
    ACC,TIME
```
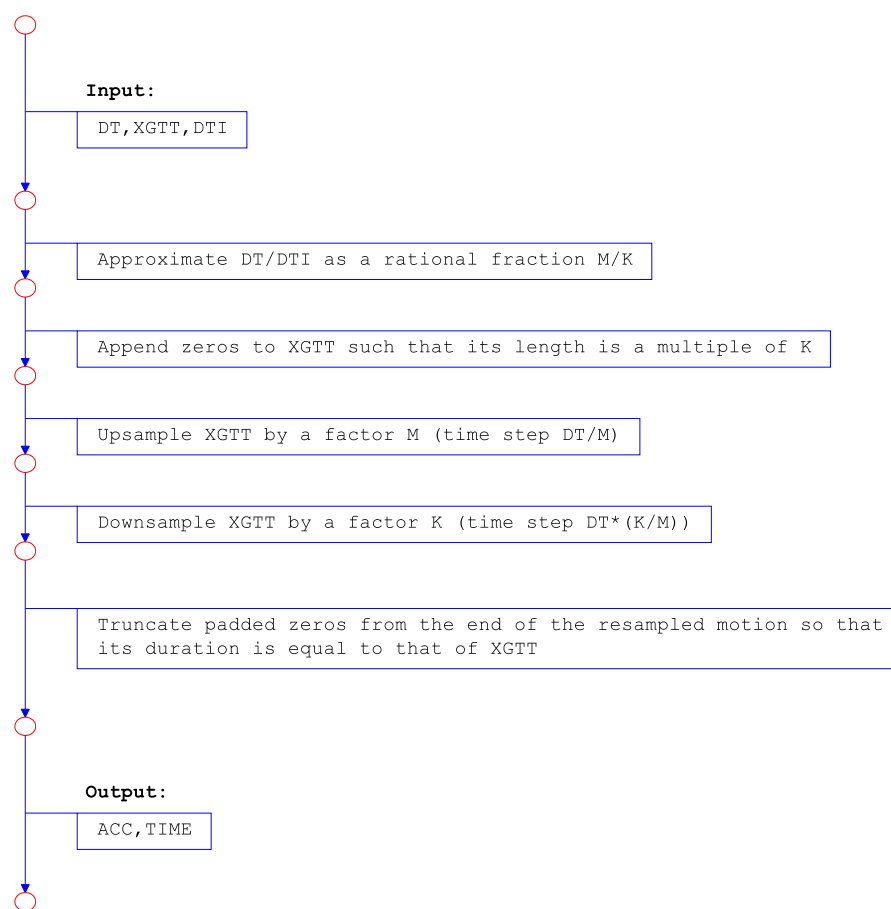
Figure 6. Flowchart for the sinc resampling procedure in OpenSeismoMatlab.

2.7. Rigid-Plastic Sliding Response Spectrum

The rigid-plastic sliding response spectrum provides the maximum response (displacement, velocity, and acceleration) of a rigid-plastic oscillator when subjected to a specific earthquake record. This response is expressed as a function of the oscillator's yield strength, represented by the ratio of its yield force to its weight, which is the sole parameter influencing its behavior.

It has been demonstrated that the maximum plastic displacement of any elastic–plastic oscillator under any earthquake excitation can be determined through a rigid-plastic oscillator. This insight has been harnessed for the assessment of elastoplastic structural responses using rigid-plastic response spectra, which are relatively simpler to formulate compared to elastic or elastoplastic spectra [27]. The rigid-plastic response spectrum can be employed to ascertain, through appropriate formulations, a realistic upper bound for the maximum plastic displacement of any elastic–plastic oscillator during a given seismic event [28]. Additionally, the rigid-plastic sliding response spectra bear relevance to the dynamic behavior of rigid block structures that rely on Coulomb friction for lateral stability [29].

Furthermore, these response spectra have served as a basis for defining the concept of equivalent motions for sliding (EMS), involving several different recorded accelerograms scaled in such a manner that the rigid-plastic response spectrum displacement remains consistent for all scaled motions, corresponding to a specific yield acceleration (or equivalently Coulomb coefficient value) [30]. Moreover, a structural design methodology for multi-story reinforced concrete shear walls has been proposed, wherein the maximum displacement is considered a dynamic performance criterion closely associated with structural damage.

From this displacement, the yield strength requirement is determined using the rigid-plastic response spectrum [31]. For an in-depth exploration of the key features and applications of rigid-plastic response spectra in seismic design, readers are referred to [32].

OpenSeismoMatlab facilitates the computation of rigid-plastic sliding response spectra using a given time-history dataset with a constant time step and a specified range of Coulomb friction coefficients, activated by the 'RPSRS' switch. The software calculates spectral displacement, velocity, and acceleration, with a detailed breakdown of the input and output parameters provided in Table 8.

Table 8. Notation, default values, and description of input and output arguments of OpenSeismoMatlab for rigid-plastic sliding response spectra ('RPSRS').

Notation	Default	Description
Input		
DT	(-) s	Time step of the input acceleration time history XGTT
XGTT	(-) m/s^2	Input acceleration time history
CF	[0.05, 0.5]	Range of Coulomb friction coefficients
Output		
SD	-	Spectral displacement
SV	-	Spectral velocity
SA	-	Spectral acceleration

Figure 7 shows the flowchart illustrating the calculation flow, i.e., the order in which the various program steps of OpenSeismoMatlab are executed for the generation of the rigid-plastic sliding response spectrum.

Input:
```
DT,XGTT,CF
```

Scan all values of friction coefficients
```
for j=1:length(CF)
```

```
Calculate the yield strength of SDOF
```

```
Calculate the dynamic response of nonlinear SDOF
```
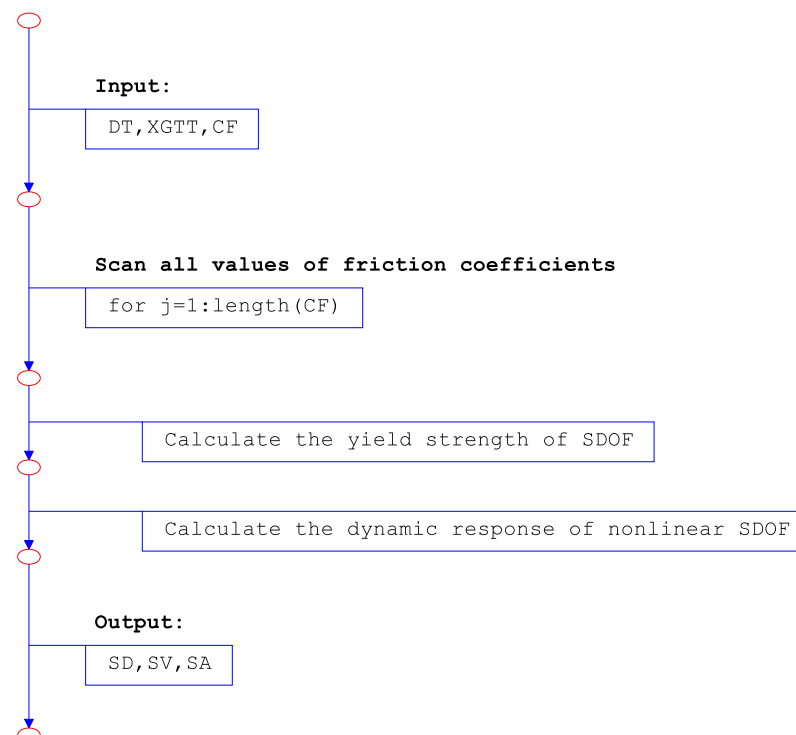
Output:
```
SD,SV,SA
```

Figure 7. Flowchart for the generation of the rigid-plastic sliding response spectrum.

3. Verification of OpenSeismoMatlab Output

This section entails the verification of various cases from the literature employing the OpenSeismoMatlab software.

3.1. High-Pass and Low-Pass Butterworth Filter of OpenSeismoMatlab

Figure 8a, taken from [7] ("Figure 1 (Left)" of that reference), displays the resulting displacements and velocities obtained through the integration of both unfiltered (gray) and filtered (high-pass with a cutoff frequency of 0.10 Hz) acceleration time history for the 1940 Imperial Valley, El Centro 9, EW earthquake. In our manuscript, any figures that are bordered, such as Figure 8a, have been sourced from external materials and included with the necessary permissions, for comparison purposes. Whenever we reference these figures using their original numbering, we denote them with quotation marks (""). The filtration process involves the use of two passes of a fourth-order high-pass Butterworth filter, which attenuates frequencies lower than the specified cutoff frequency, mirroring the approach adopted in OpenSeismoMatlab via the 'BUTTERWORTHHIGH' switch. The corresponding results of OpenSeismoMatlab are shown in Figure 8b. In the third sub-figure of Figure 8a, the displacement axis labels for the unfiltered motion are provided on the right side. As depicted in this figure, the unfiltered displacement exhibits values near zero at the conclusion of the motion, a circumstance that is coincidental and uncommon; in most instances, displacements resulting from unfiltered accelerations deviate significantly from zero at the record's conclusion, as illustrated by the 1999 recording shown at the right part of the figure.
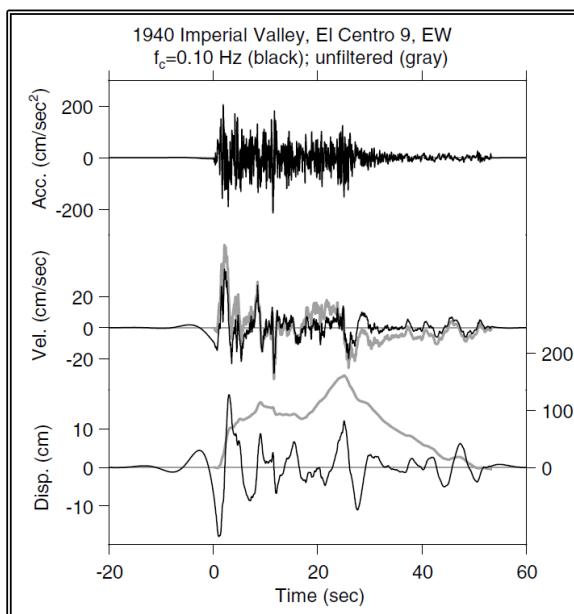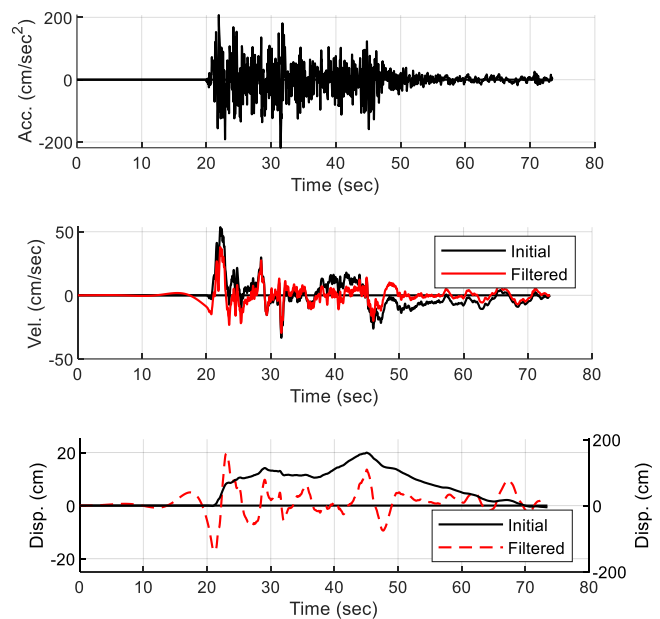
(**a**) (reproduced with permission) (**b**)

Figure 8. Verification of the high-pass Butterworth filter of OpenSeismoMatlab: (**a**) "Figure 1 (Left)" of [7], (**b**) corresponding results of OpenSeismoMatlab.

To validate not only the high-pass but also the low-pass filters integrated into OpenSeismoMatlab, we reference "Figure 3.2a" from [25] for verification. This validation process pertains to the MW 6.3 earthquake in Christchurch, New Zealand, specifically at the Heathcote Valley Primary School (HVSC) station, Up-component. Figures 9–12 present a comparison between the time histories, Fourier spectra, and elastic response spectra derived from unfiltered and filtered accelerations.
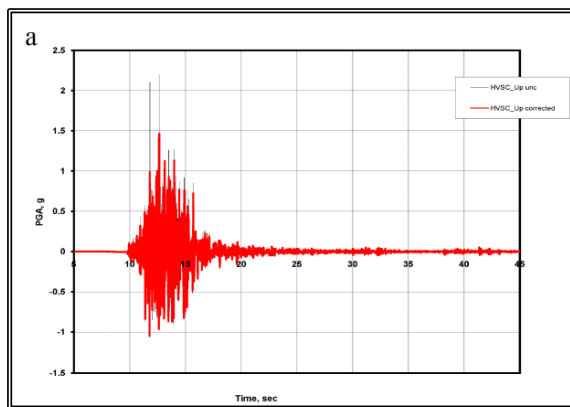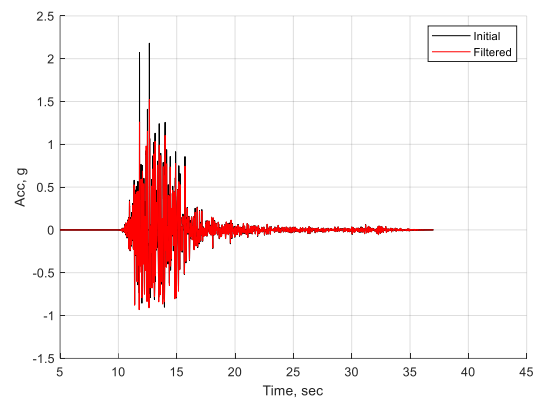
(**a**) (reproduced with permission)　　　　　　　　　　(**b**)

Figure 9. Uncorrected and corrected acceleration time histories of the MW 6.3 Christchurch, New Zealand earthquake at Heathcote Valley Primary School (HVSC) station, Up-component: (**a**) "Figure 3.2a" of [25], (**b**) corresponding results of OpenSeismoMatlab.
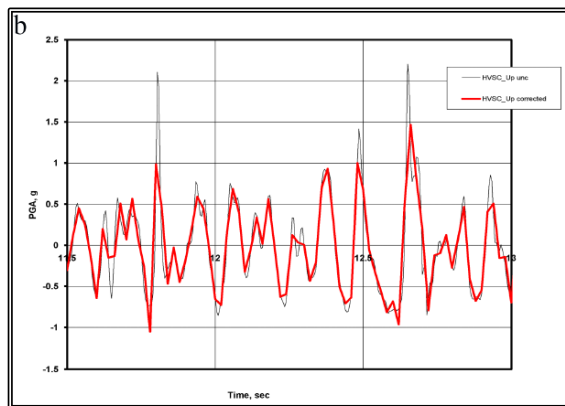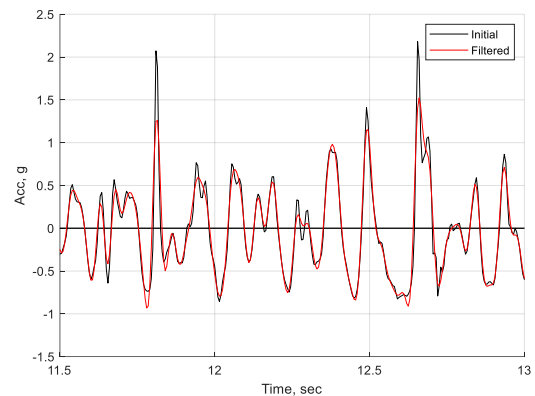
(**a**) (reproduced with permission)　　　　　　　　　　(**b**)

Figure 10. Uncorrected and corrected acceleration time histories of the MW 6.3 Christchurch, New Zealand earthquake at Heathcote Valley Primary School (HVSC) station, Up-component for the time range from 11.5 s to 13 s: (**a**) "Figure 3.2b" of [25], (**b**) corresponding results of OpenSeismoMatlab.
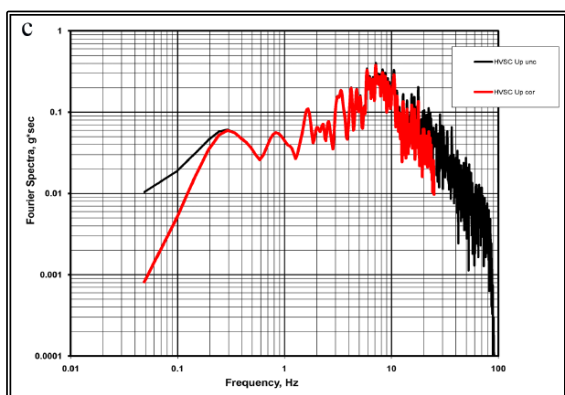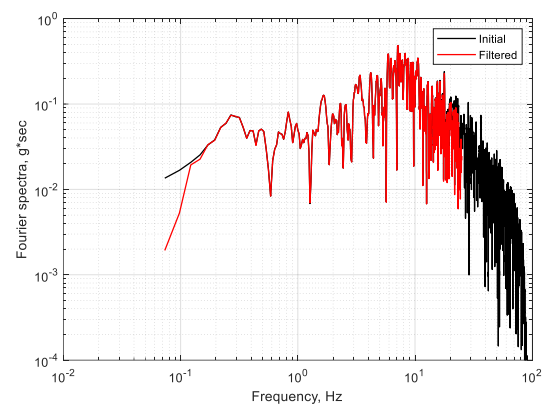
(**a**) (reproduced with permission)　　　　　　　　　　(**b**)

Figure 11. Fourier amplitude spectra of uncorrected and corrected acceleration time histories of the MW 6.3 Christchurch, New Zealand earthquake at Heathcote Valley Primary School (HVSC) station, Up-component: (**a**) "Figure 3.2c" of [25], (**b**) corresponding results of OpenSeismoMatlab.

(**a**) (reproduced with permission)   (**b**)
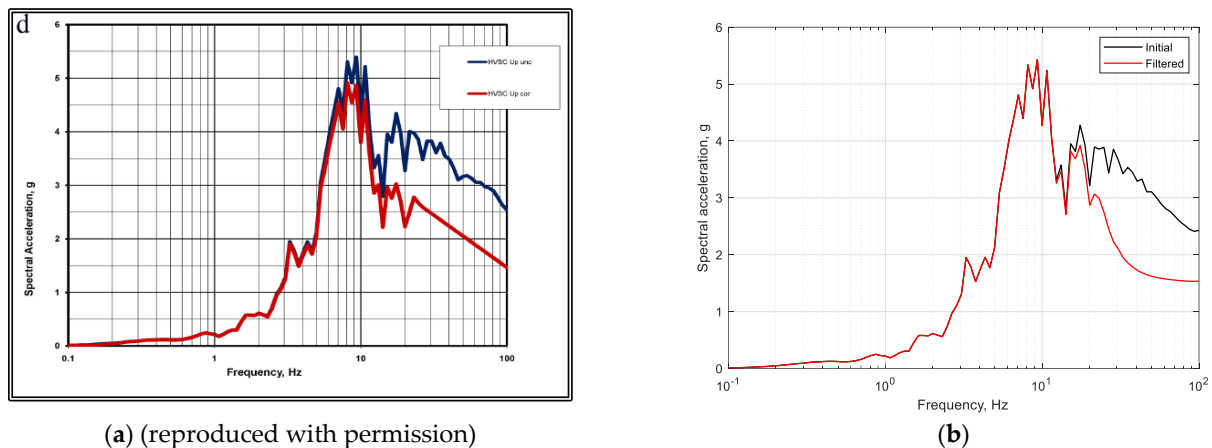
Figure 12. Elastic response spectra of uncorrected and corrected acceleration time histories of the MW 6.3 Christchurch, New Zealand earthquake at Heathcote Valley Primary School (HVSC) station, Up-component: (**a**) "Figure 3.2d" of [25], (**b**) corresponding results of OpenSeismoMatlab.

In the aforementioned study, ground motion underwent processing following the 1970s Caltech procedure. It was subsequently low-pass filtered and resampled at a rate of 50 samples per second by the GeoNet New Zealand strong motion network. In contrast, the present study applies a Butterworth filter with a high-pass cutoff frequency of 0.1 Hz and a low-pass cutoff frequency of 25 Hz. Evidently, the latter filtering approach employed by OpenSeismoMatlab yields comparable results.

Figure 9 displays the time histories of both the original and filtered motions. A closer examination of the time range between 11.5 and 13 s, where the most significant acceleration peaks occur, is presented in Figure 10. Figure 11 showcases the Fourier amplitude spectra of the initial and filtered motions, revealing lower amplitudes in the spectrum of the filtered motion for frequencies below 0.1 Hz (the high-pass cutoff frequency) and above 25 Hz (the low-pass cutoff frequency). This observation corroborates the accuracy of OpenSeismoMatlab's filtering procedure. Furthermore, the overall configuration of the spectra closely aligns with the corresponding results from [25].

Figure 12 provides linear elastic response spectra for both the unfiltered and corrected motions. Notably, the spectral acceleration at high frequencies is lower than that of the uncorrected motion, which is consistent with the trends observed in "Figure 3.2d" of [25].

3.2. Constant Ductility Response Spectra of OpenSeismoMatlab (CDRS)

We have replicated the constant ductility response spectra featured in "Figure 7.5.2" of [33] (not reproduced here due to copyright restrictions) using OpenSeismoMatlab. These response spectra pertain to elastoplastic systems with ductility demands μ = 1, 1.5, 2, 4, and 8, all of which exhibit a damping ratio ζ = 5%. These systems are subjected to the El Centro ground motion record of the Imperial Valley, California earthquake of May 18, 1940. The spectra, which have been calculated using OpenSeismoMatlab, are presented in Figure 13.

Our observations reveal that the yield strength f_y required for an SDOF system to undergo nonlinear response is lower than the minimum strength required for the system to exhibit linear elastic behavior. Additionally, we note that as the target ductility factor increases, the necessary yield strength decreases. The most significant reduction in yield strength appears to occur between μ = 1 and μ = 1.5, corresponding to the transition from linear elastic behavior to a case with minimal ductility demands. Notably, the results depicted in Figure 13 exhibit remarkable similarity to the corresponding results shown in "Figure 7.5.2" of [33], underscoring the high level of accuracy in OpenSeismoMatlab's output.
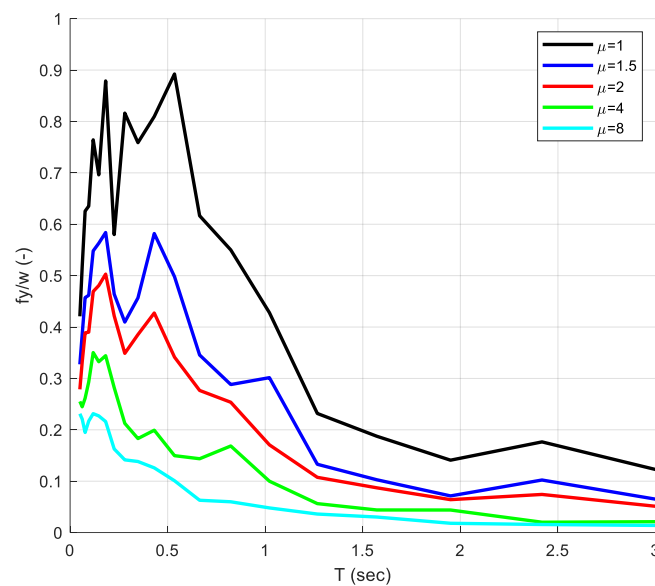
Figure 13. Constant ductility response spectra of the Imperial Valley, California earthquake of May 18, 1940, El Centro record, NS component.

Figure 14 displays the constant ductility response spectra for the North–South component of the Imperial Valley irrigation substation record, captured during the Imperial Valley, California earthquake on 18 May 1940. This is illustrated for constant ductility factors μ = 1, 2, and 4, along with a critical damping ratio ξ = 0.02. The outcomes derived from OpenSeismoMatlab for these parameters are juxtaposed with the results depicted in "Figure 12.18" of [34]. Notably, there is a pronounced concordance between these two sets of results. This is particularly noteworthy given that multiple strength values (i.e., of the constant ductility spectrum) may be associated with a single combination of eigenperiod and ductility factor. It is observed that strength decreases for low and diminishing eigenperiod values (below 0.2 s), regardless of the ductility factor. Additionally, it is evident that an increase in ductility demand leads to a reduction in the constant ductility response spectra, aligning with expectations. The high degree of similarity between the results further reaffirms the accuracy and reliability of OpenSeismoMatlab.

(**a**) (reproduced with permission)

(**b**)
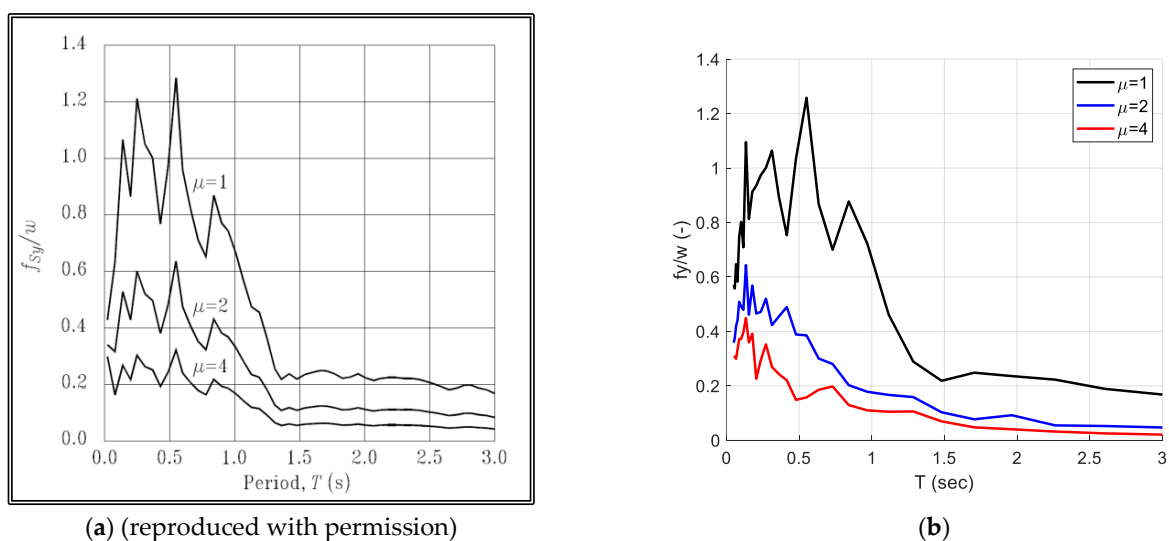
Figure 14. Constant ductility response spectra of the Imperial Valley, California earthquake of May 18, 1940, a record of irrigation substation in El Centro, NS component, for constant ductility factors μ = 1,2 and 4, for ξ = 0.02: (**a**) "Figure 12.18" of [34], (**b**) corresponding results of OpenSeismoMatlab.

3.3. Constant Strength Response Spectra of OpenSeismoMatlab (CSRS)

In [35], a novel spectrum known as the constant strength response spectrum (CSRS) was introduced, along with a displacement ductility demand spectrum (DDDS) that establishes a relationship between peak displacement ductility demands, as well as other significant response parameters such as displacements, and the structural periods of nonlinear elastic–perfectly plastic hysteretic SDOF systems with predetermined yield strengths. In this section, we validate the findings presented in Figure 1 of the aforementioned reference using OpenSeismoMatlab.

The SDOF system under consideration features a yield strength ratio (i.e., yielding shear force divided by the structure weight, V/W) of V/W = 0.15. We employ the acceleration time history of the SCT-EW component recorded during the 1985 Michoacán earthquake. Figures 14 and 15 illustrate the ductility demand and displacement demand, respectively, plotted against the eigenperiod of the SDOF oscillator. Both the outcomes published in reference [35] and those generated by OpenSeismoMatlab exhibit a substantial level of agreement.

(a) (reproduced with permission)   **(b)**
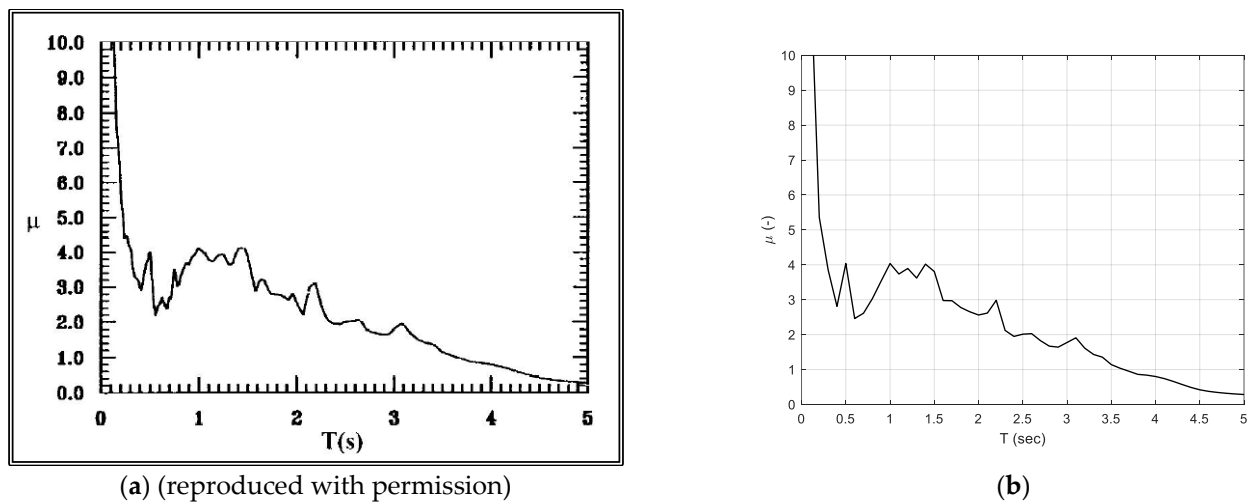
Figure 15. Displacement ductility demand spectra (or CSRS) for a structural system with V/W = 0.15 subjected to the 1985 Michoacán SCT-EW record: (**a**) "Figure 1 (Left)" of [35], (**b**) corresponding results of OpenSeismoMatlab.

Figure 15 demonstrates that for a given yield strength ratio V/W, there is a notable increase in ductility demand as the structure becomes stiffer, resulting in a decrease in its eigenperiod. Conversely, softer structures exhibit a contrasting trend. It is evident from Figure 15 that there exists a limiting eigenperiod beyond which the structure behaves in a linear elastic manner, as the ductility demand appears to fall below unity.

In Figure 16, the displacement demand reaches its maximum value at an eigenperiod of approximately 3 s. For eigenperiod values less than 3 s, the displacement demand rises with increasing eigenperiod, whereas for eigenperiod values exceeding 3 s, the displacement demand decreases as the eigenperiod increases.

The concept of the constant strength response spectrum (CSRS), as initially introduced in [35], was further expanded upon in [12]. The latter publication introduces an integral method for the seismic assessment of existing structures, utilizing the displacement ductility demand spectrum (DDDS), which is equivalent to the CSRS. In this section, we validate the findings presented in Figure 1 of the referenced work. In this verification, the SDOF system features a yield strength ratio of V/W = 0.10, and we employ the acceleration time history of the SCT-EW component recorded during the 1985 Michoacán earthquake. Figures 16 and 17 depict the results obtained, showcasing a notable agreement between the corresponding outcomes of [12] and OpenSeismoMatlab. It is worth noting that the same trends observed in Figures 14 and 15 are also apparent in Figures 17 and 18, respectively.
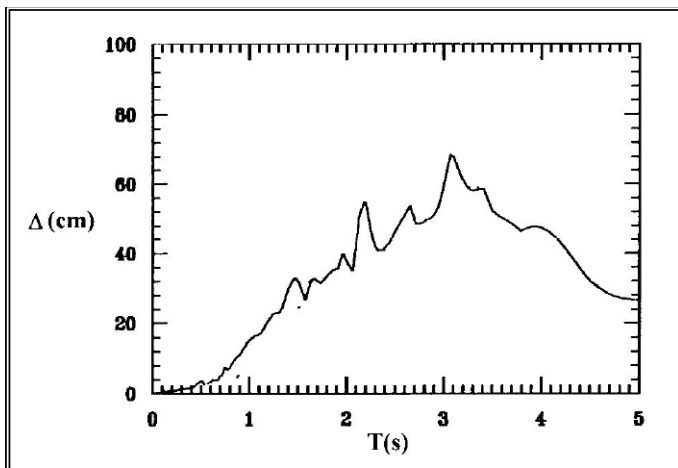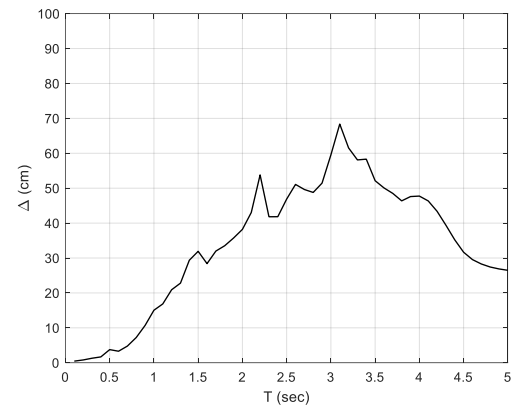
(**a**) (reproduced with permission)　　　　　　　　　　　　　　　　　(**b**)

Figure 16. Displacement ductility demand spectra (or CSRS) for a structural system with V/W = 0.15 subjected to the 1985 Michoacán SCT-EW record: (**a**) "Figure 1 (Right)" of [35], (**b**) corresponding results of OpenSeismoMatlab.
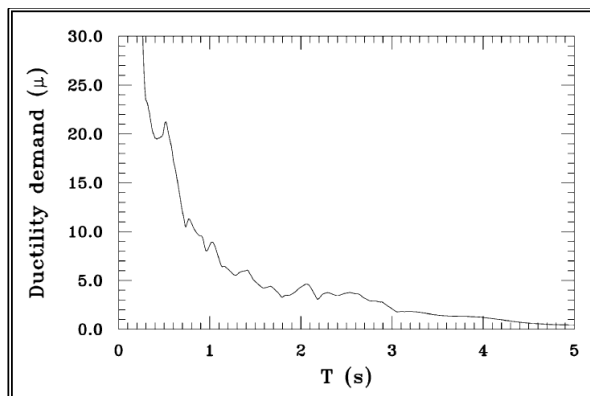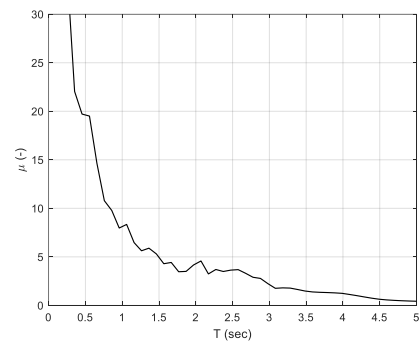
(**a**) (reproduced with permission)　　　　　　　　　　　　　　　　　(**b**)

Figure 17. Ductility demand spectra for an elastic–perfectly plastic system with a base shear ratio V/W = 0.10, subjected to the 1985 Michoacán SCT-EW acceleration record: (**a**) "Figure 1 (Left) of [12], (**b**) corresponding results of OpenSeismoMatlab.
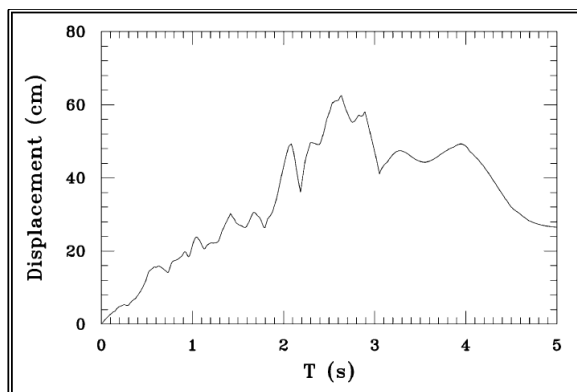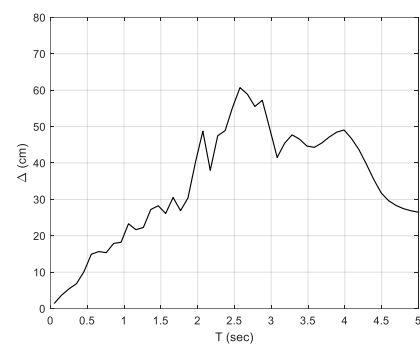
(**a**) (reproduced with permission)　　　　　　　　　　　　　　　　　(**b**)

Figure 18. Displacement demand spectra for an elastic–perfectly plastic system with a base shear ratio V/W = 0.10, subjected to the 1985 Michoacán SCT-EW acceleration record: (**a**) "Figure 1 (right)" of [12], (**b**) corresponding results of OpenSeismoMatlab.

3.4. Incremental Dynamic Analysis of OpenSeismoMatlab (IDA)

In a prior study [36], incremental dynamic analysis (IDA) was conducted for a non-degrading single-degree-of-freedom (SDOF) model characterized by an eigenperiod of T = 1 s. The analysis employed a bilinear elastoplastic hysteresis model tailored for non-degrading SDOF systems, illustrated in "Figure 17a" within the same reference. The IDA was performed utilizing a ground motion signal with spectral acceleration akin to the red line delineated in "Figure 14" of that reference, specifically targeting Sa (1 s) = 0.382 g as the intensity measure (IM). Additionally, the ground motion sought to emulate a duration $D_{5\text{–}75}$ roughly equivalent to 8.3 s, as visualized in "Figure 16c" of [36]. For the purpose of this section's verification, an arbitrary ground motion acceleration waveform was initially selected. Subsequently, this waveform was meticulously adjusted to ensure that the resulting time history adhered to the stipulated criteria of Sa(1 s) = 0.382 g and $D_{5\text{–}75} \approx 8.3$ s. Based on this verification case, the median response curve depicted in "Figure 18a" of reference [36] is scrutinized in the ensuing Figure 19. Here, the blue curve in Figure 19a is juxtaposed with the curve featured in Figure 19b. It is worth noting that the blue curve signifies the median response curve, predicated on the blue scattered data points associated with the responses of a non-degrading SDOF model boasting an eigenperiod of 1 s, subjected to an array of ground motions. Within the current study, an arbitrary ground acceleration time history was handpicked, differing from the ground motions appraised in [36], with the aim of replicating the outcomes delineated in "Figure 18a" of the same reference. Consequently, it is anticipated that the alignment between the outcomes of [36] and those generated by OpenSeismoMatlab may not achieve perfect congruence, given the nuanced selection of ground motion signals. However, despite the inherent disparities in the data sources, the general configuration of the two curves compared in Figure 19 illustrates a commendable degree of alignment and agreement.

(a) (reproduced with permission) **(b)**
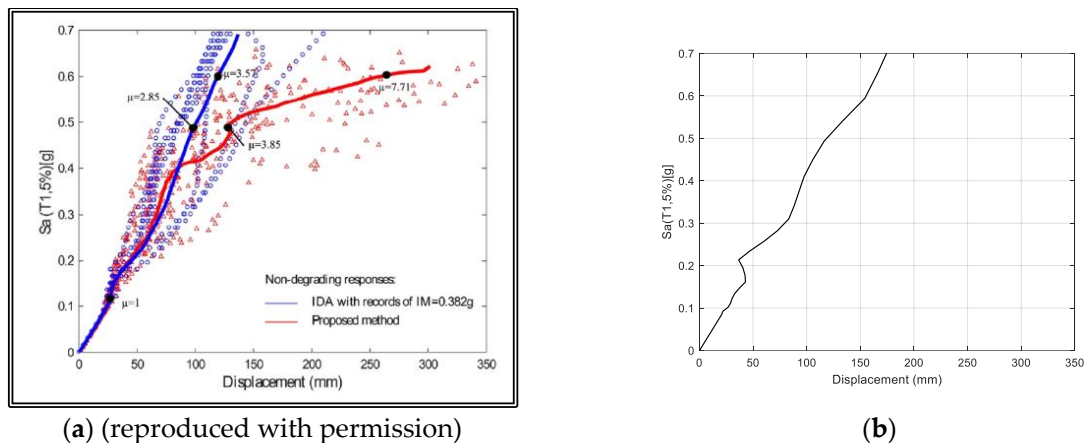
Figure 19. Median response IDA curves for a non-degrading SDOF model with eigenperiod equal to 1 s: (**a**) "Figure 18a" of [36], (**b**) corresponding results of OpenSeismoMatlab.

In "Figure 4a" of the reference [37], a set of incremental dynamic analysis (IDA) curves illustrates the responses of an elastoplastic single-degree-of-freedom (SDOF) system subjected to the Consortium of Universities for Research in Earthquake Engineering (CUREE) ground motion (GM) suite [38], with the curves constructed based on maximum acceleration. This section focuses on the utilization of OpenSeismoMatlab to generate IDA curves employing a deliberately chosen suite of robust ground motion records. In Figure 20, the IDA curves closely mirror those presented in "Figure 4a" of [37] (not reproduced here due to copyright restrictions), particularly evident in the median IDA curve represented in red. It should be noted that while the IDA curves exhibit a strong resemblance, a degree of variation is evident among them. This discrepancy arises primarily from the random selection of the suite of strong ground motions employed in the present verification study.

Given the stochastic nature of the ground motion selection, some differences in the IDA curves are anticipated as an inherent outcome of this approach.
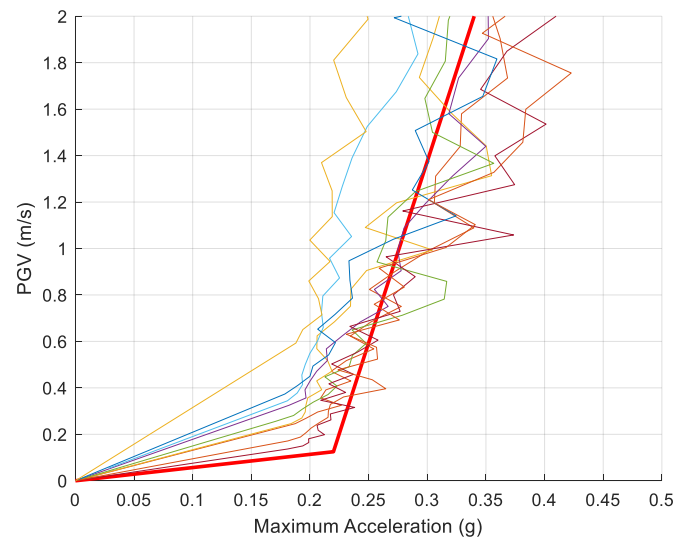
Figure 20. IDA curves of an elastoplastic SDOF system from an arbitrarily selected ground motion suite, using OpenSeismoMatlab.

In "Figure 1b" of the reference [39], which is also depicted in Figure 21 below, the median incremental dynamic analysis (IDA) curves for single-degree-of-freedom (SDOF) systems with an eigenperiod of T = 0.5 s are presented. In the same study, "Figure 1a" displays the actual capacity curve of the SDOF oscillator (illustrated as the green line), which has been approximated by an elastoplastic bilinear fit following FEMA-440 guidelines (depicted as the blue line). This fitting process introduces a discernible error or bias, depicted as the blue shaded area in "Figure 1b", which is generally conservative. For the current investigation, two arbitrary acceleration time histories are thoughtfully selected, and IDA curves for displacement response are constructed. These IDA curves are established based on an SDOF system featuring carefully chosen properties derived from "Figure 1a". As evident in Figure 21, both curves roughly align with the bias region (blue area) observed in "Figure 1b" of the previously mentioned reference.
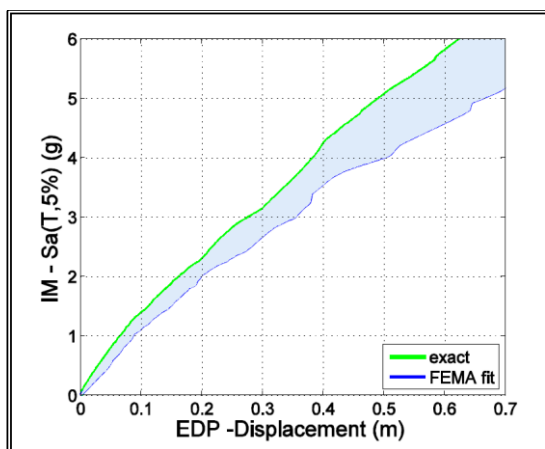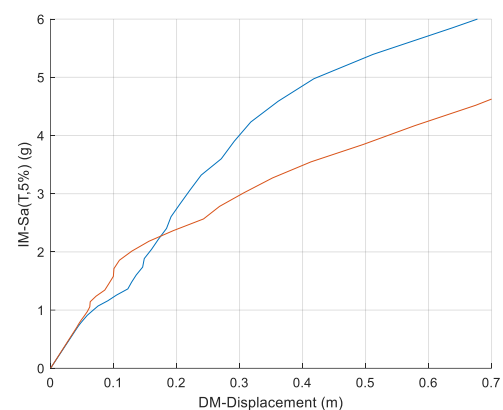
(**a**) (reproduced with permission)　　　　　　　　　　　　　　　　　(**b**)

Figure 21. Median IDA curves showing the negative (conservative) bias due to elastoplastic bilinear fitting according to FEMA-440 for T = 0.5 s: (**a**) "Figure 1b" of [39], (**b**) corresponding results of OpenSeismoMatlab.

It is noted that the IDA analysis provided by OpenSeismoMatlab is related to only SDOF systems, the response of which may not always reflect the response of actual structures that involve multiple degrees of freedom. While the IDA analysis performed by OpenSeismoMatlab may yield accurate results for regular structures that are less sensitive to torsion and localized plasticity, it may not be comprehensive enough for structures with asymmetry either in plan or in elevation. In fact, nonlinear elastoplastic analysis of SDOF systems such as that offered by OpenSeismoMatlab has proven to be quite accurate for regular structures. However, for structures exhibiting asymmetry, especially regarding the plan and elevation, a more comprehensive approach is necessary, and the presented IDA capability may not adequately address the complexities of analyzing such structures. This issue can be resolved by implementing appropriate modifications in the IDA analysis of OpenSeismoMatlab, so that structural symmetries are taken into account while processing an acceleration time history and will be considered in future studies by the authors. Other remedies for this could be the development of other improved analytical methods or enhancing existing ones to accurately predict seismic responses in asymmetric structures, while at the same time revisiting the various basic assumptions involved in such analyses.

3.5. Pulse Decomposition of OpenSeismoMatlab

In order to verify OpenSeismoMatlab's pulse extraction capability, the velocity pulse within the velocity time history of the fault-normal component recorded during the 1994 Northridge earthquake at Rinaldi is extracted, following the procedure detailed in "Figure 4" of reference [20]. Specifically, the Daubechies wavelet of order 4, as depicted in "Figure 2c" of the aforementioned reference, serves as the mother wavelet. The extraction process begins by identifying the largest velocity pulse, as visualized in "Figure 4a" of [20] and also presented in Figure 22a of the present study. Subsequently, this identified pulse is subtracted from the original ground motion. From the resulting residual motion, it becomes possible to identify and subtract the largest velocity pulse, which coincides with the second-largest velocity pulse in the original motion. This iterative procedure allows for the decomposition of any given velocity time history into a sum of pulses represented by Daubechies wavelets. Once again, it is noteworthy that a substantial level of agreement is observed between the corresponding outcomes obtained from [20] and those generated by OpenSeismoMatlab.
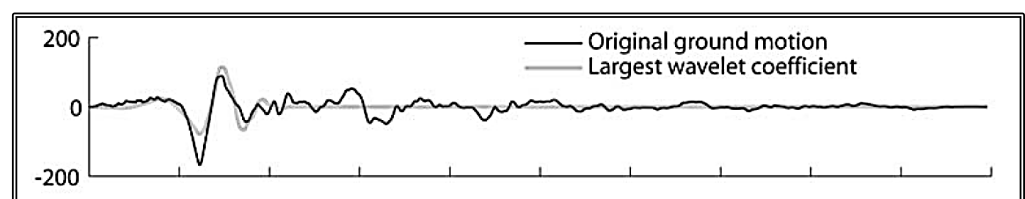
(a) (reproduced with permission)
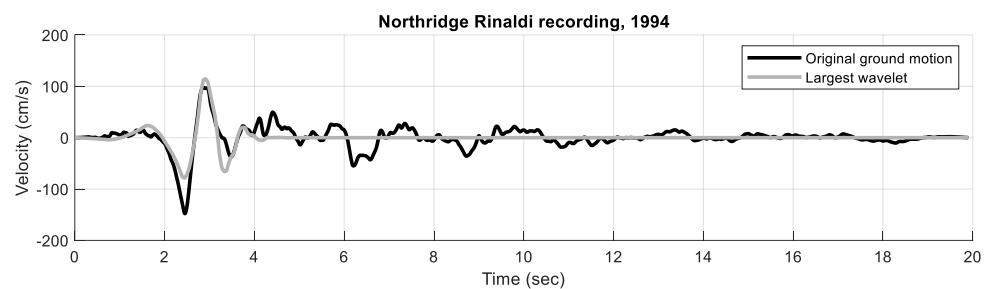
(b)

Figure 22. Illustration of the decomposition procedure used to extract the pulse portion of a ground motion (the fault-normal component of the 1994 Northridge, Rinaldi, recording): (**a**) "Figure 4a" of [20], (**b**) corresponding results of OpenSeismoMatlab.

In "Figure 3" of reference [40], the velocity time history derived from the 1979 Imperial Valley El Centro Array 4 recording undergoes a deconstruction process into 30 wavelets using a continuous wavelet transform. Following this procedure, the 30 wavelets are subsequently aggregated to reconstruct the ground motion, offering an approximation of the original ground motion. The outcomes from the aforementioned reference, along with those produced by OpenSeismoMatlab, are presented in Figure 23 below. The Daubechies wavelet of order 4 serves as the mother wavelet for this analysis. Notably, a considerable level of concordance emerges between the original and the reconstructed ground motions. The results indicate that pulse-like ground motions are chiefly characterized by a small number of potent wavelets. Furthermore, there is a conspicuous alignment between the corresponding findings of [40] and OpenSeismoMatlab, affirming the software's efficacy in reproducing these results.
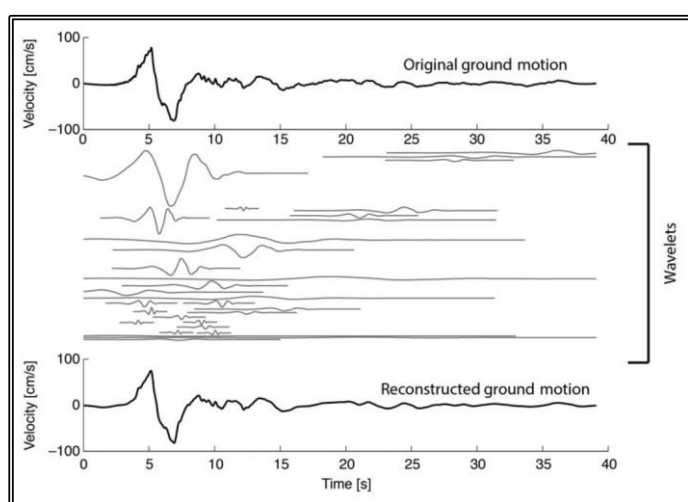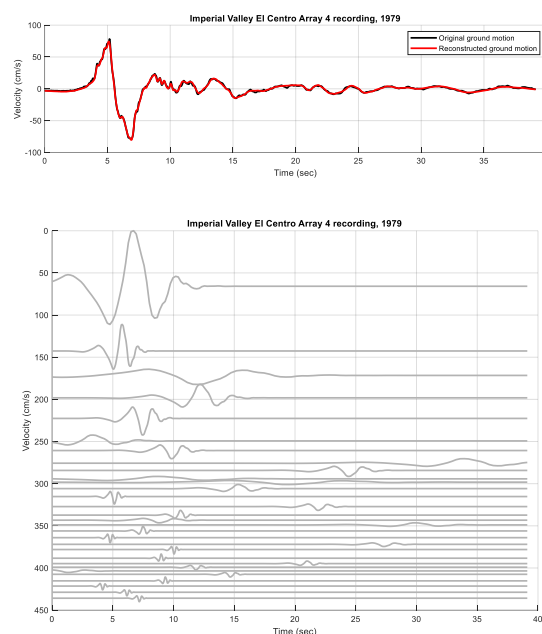
(**a**) (reproduced with permission)   (**b**)

Figure 23. Decomposition and reconstruction of the El Centro Array 4 velocity time history recording, from the 1979 Imperial Valley earthquake. Original motion, reconstructed motion, and wavelets: (**a**) "Figure 3" of [40], (**b**) corresponding results of OpenSeismoMatlab.

3.6. Rigid-Plastic Sliding Response Spectrum of OpenSeismoMatlab

"Figure 6" of reference [29] presents the symmetric sliding spectra for a collection of Greek ground motions, encompassing records such as Chavriata (EW), Lixouri (EW), and Lixouri (NS) from the February 2014 Cephalonia, Greece earthquake event (3 Feb 2014, 13:34 EST). OpenSeismoMatlab is utilized to compute the rigid-plastic sliding response spectra for these three specific records. The acceleration time histories used for spectrum extraction are featured in "Figure 2" of [29], specifically Chavriata (3 February) EW, Lixouri (3 February) EW, and Lixouri (3 February) NS. In the calculation of the sliding response spectra, the oscillator is assumed to exhibit ideal rigid-plastic sliding on a horizontal plane, as depicted in "Figure 4a" of [29]. The outcomes from "Figure 6" of reference [29] and OpenSeismoMatlab are presented in Figure 24. It should be noted that while the aforementioned reference accounts for both the horizontal and vertical components of various records, OpenSeismoMatlab exclusively considers the horizontal component. Consequently, some distinctions may arise between the results of the reference and those from OpenSeismoMatlab. However, despite these differing approaches, a notable degree of alignment appears to exist between the respective findings.
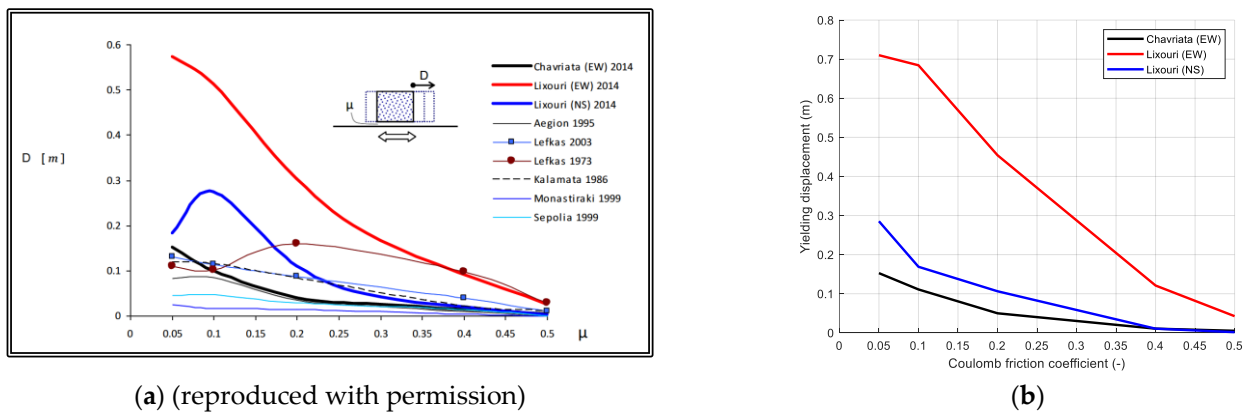
(**a**) (reproduced with permission)

(**b**)

Figure 24. Sliding response spectra in terms of yielding displacement, D, versus the coefficient of friction, μ, for Chavriata (EW), Lixouri (EW), and Lixouri (NS) records from the February 2014 Cephalonia, Greece earthquake event: (**a**) "Figure 6" of [29], (**b**) corresponding results of OpenSeismoMatlab.

Rigid-plastic sliding response spectra are derived for two distinct acceleration time histories: the Northridge (Sylmar County), January 1994 record, and the El Centro, NS, May 1940 record, as documented in "Table 1" of reference [28]. This analysis assumes the oscillator to be an idealized rigid-plastic slider on a horizontal plane. Figure 25 offers a comparative evaluation between the rigid-plastic sliding response spectra obtained via OpenSeismoMatlab and those featured in "Figure 6" of the aforementioned reference. The congruence between the corresponding outcomes is evident and substantiates the reliability of the results.
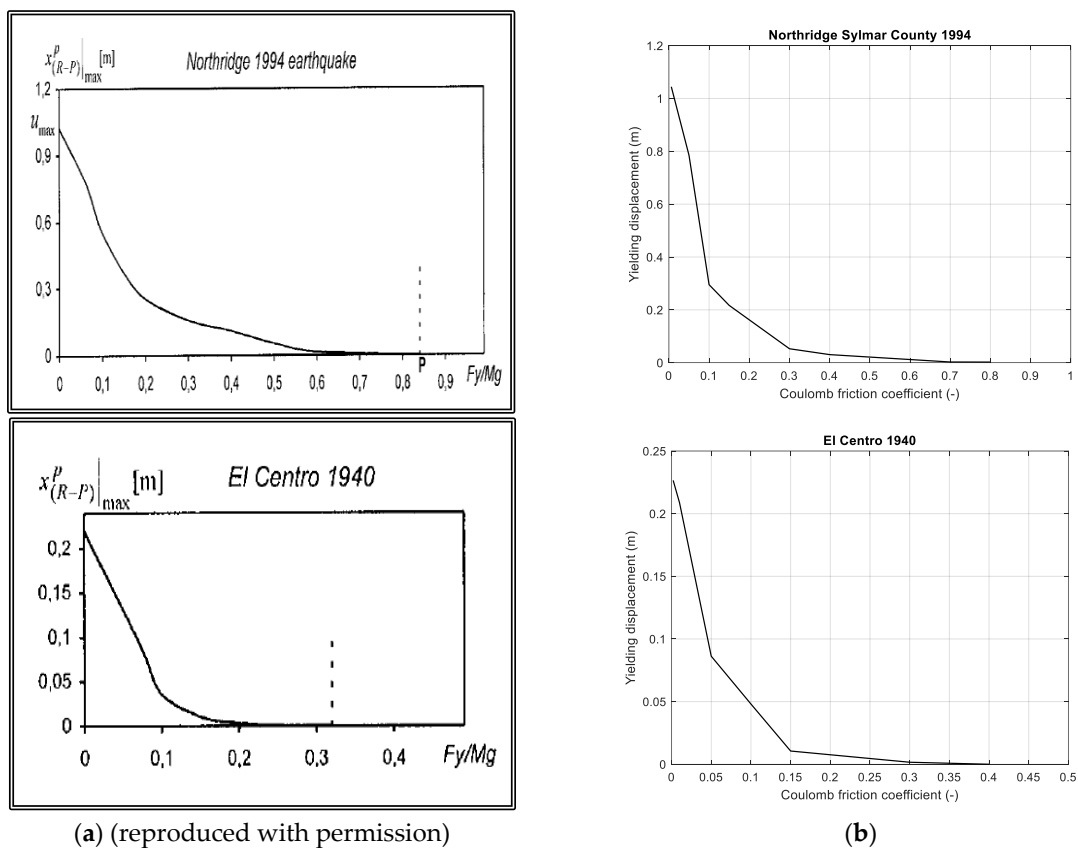
(**a**) (reproduced with permission)

(**b**)

Figure 25. Rigid-plastic spectra for Northridge 1994 and El Centro 1940 earthquakes: (**a**) "Figure 6" of [28], (**b**) corresponding results of OpenSeismoMatlab.

4. Discussion and Future Work

Throughout the preceding section, it becomes evident that the outcomes generated by OpenSeismoMatlab closely align with the corresponding findings presented in the existing body of literature. In instances where perfect congruence is not achieved, any disparities observed can be reasonably attributed to specific assumptions forming the basis of the calculations. Among these, two pivotal assumptions underpinning OpenSeismoMatlab are as follows:

- OpenSeismoMatlab exclusively employs the bilinear kinematic model for conducting nonlinear analyses, encompassing a range of nonlinear spectra, including constant ductility, constant strength, and rigid-plastic sliding spectra.
- The general single step single solve (GSSSS) integration algorithm [41,42] serves as the chosen method for executing the time integration of the dynamic equations of motion within the software.

It should be noted that the GSSSS time integration algorithm represents a generalized version of most well-established time integration algorithms, with the latter serving as specific cases within the GSSSS family. For a comprehensive exposition, interested readers are directed to reference [42]. The commendable concurrence evident in the verification section of this study substantiates OpenSeismoMatlab's standing as a precise and dependable software for processing strong ground motion data, with higher accuracy compared to alternative strong ground motion processing software (see [1] for example). Furthermore, in contrast to its earlier iterations, OpenSeismoMatlab has undergone extensive refactoring, resulting in a revised format for input arguments structured as "time step"—"time history"—"switch." This adaptation not only paves the way for further software development but also facilitates enhancement through the selection of an appropriate string as the "switch," enabling the incorporation of desired functionalities. Consequently, the software's potential for augmentation has been significantly expanded.

In addition to the aforementioned considerations, future research endeavors could encompass the development of seismic design methodologies that incorporate multiple outputs generated by OpenSeismoMatlab. For instance, a judicious amalgamation of the linear elastic response spectrum and the rigid-plastic sliding response spectrum derived from a given acceleration time history could be employed in the seismic design of ductile structures, as opposed to the prevailing practice of exclusively relying on the linear elastic response spectrum, even for structures exhibiting nonlinear behavior. The inadequacy of elastic response spectra for designing ductile structures has been underscored in prior work [30]. Nevertheless, the realm of research should extend beyond specific spectra of quantifiable parameters for assessing the seismic impact on structures.

Moreover, the data yielded by OpenSeismoMatlab (or any analogous software for strong ground motion processing) could be harnessed through advanced AI techniques, such as artificial neural networks. These methods have the potential to unveil optimal strategies for amalgamating and further processing these output parameters, thereby elucidating pathways for enhanced seismic impact assessment [43,44]. With the advent of AI and with continuously increasing computational power, it is apparent that OpenSeismoMatlab can contribute to the development of more advanced AI tools, or obtain some benefits from such modern technologies [45]. For example, machine learning (ML) can be used for training models that will be able to identify patterns between seismic inputs (acceleration time histories) and outputs (e.g., various spectra). OpenSeismoMatlab could be used for providing training data for ML models. In addition, ML techniques can be employed to analyze structural responses obtained from OpenSeismoMatlab and detect patterns that can be used for improving structural design. Patterns can be detected not only in time histories, but also in the frequency domain, or in a combination of the two. Furthermore, AI tools may be used for proper interpolation of earthquake data which can largely reduce the computational demand and thus make software run faster. Moreover, OpenSeismoMatlab can pave the way for the development of AI models to handle uncertainties in seismic

data (time histories, spectra, or other parameters) and provide more robust predictions and simulations.

5. Conclusions

In this study, we have provided a detailed description of the most recent version of OpenSeismoMatlab, a software tool designed for the processing of strong ground motion data, specifically tailored for the evaluation and design of buildings and various other structures. Furthermore, we have conducted a comprehensive verification process by comparing the software's results to a selection of cases documented in the existing literature. Our findings have unequivocally established OpenSeismoMatlab as a dependable and precise tool for strong ground motion processing. Furthermore, it is worth mentioning that OpenSeismoMatlab can provide more accurate results compared to other software for processing strong ground motion. This superiority arises from the utilization of the generalized single step single solve time integration algorithms within OpenSeismoMatlab, giving it an edge over alternative options. Notably, the software boasts a straightforward and user-friendly conceptual design, facilitating ease of use. It is also noteworthy that the software's existing framework allows for seamless integration of additional functionalities. Future research endeavors may focus on optimizing the utilization of OpenSeismoMatlab's outputs to enhance the realism of earthquake impact assessments on structures.

Author Contributions: Conceptualization, G.P.; methodology, G.P.; software, G.P.; validation, V.P. and G.P.; formal analysis, V.P.; investigation, V.P.; writing—original draft preparation, G.P.; writing—review and editing, V.P.; supervision, V.P. All authors have read and agreed to the published version of the manuscript.

Data Availability Statement: All data relevant to this work can be found in the online repository https://github.com/GeorgePapazafeiropoulos/OpenSeismoMatlab (accessed on 18 January 2024). All the examples presented in this study can be found in the "lib" subfolder of the repository. The "doc" subfolder contains the entire documentation of OpenSeismoMatlab in PDF format. The "tlbx" subfolder contains the OpenSeismoMatlab software in toolbox format, which, if installed in Matlab software, enables the use of the various subfunctions of OpenSeismoMatlab within Matlab as an expanded functionality. An online version of the documentation of OpenSeismoMatlab is provided at https://georgepapazafeiropoulos.github.io/html/Contents_.html (accessed on 18 January 2024).

Conflicts of Interest: The authors declare no conflicts of interest.

References

1. Papazafeiropoulos, G.; Plevris, V. OpenSeismoMatlab: A new open-source software for strong ground motion data processing. *Heliyon* **2018**, *4*, e00784. [CrossRef] [PubMed]
2. Papazafeiropoulos, G.; Plevris, V. Kahramanmaraş—Gaziantep, Türkiye Mw 7.8 Earthquake on 6 February 2023: Strong Ground Motion and Building Response Estimations. *Buildings* **2023**, *13*, 1194. [CrossRef]
3. Papazafeiropoulos, G.; Plevris, V.; Papadrakakis, M. A new energy-based structural design optimization concept under seismic actions. *Front. Built Environ.* **2017**, *3*, 1–16. [CrossRef]
4. Housner, G.W. Spectrum Intensities of Strong-Motion Earthquakes. In *Symposium on Earthquake and Blast Effects on Structures*; Earthquake Engineering Research Institute: Los Angeles, CA, USA, 1952.
5. Nau, J.M.; Hall, W.J. Scaling Methods for Earthquake Response Spectra. *J. Struct. Eng.* **1984**, *110*, 1533–1548. [CrossRef]
6. Gustafsson, F. Determining the initial states in forward-backward filtering. *IEEE Trans. Signal Process.* **1996**, *44*, 988–992. [CrossRef]
7. Boore, D.M. On Pads and Filters: Processing Strong-Motion Data. *Bull. Seismol. Soc. Am.* **2005**, *95*, 745–750. [CrossRef]
8. Chanerley, A.A.; Alexander, N.A. Obtaining estimates of the low-frequency 'fling', instrument tilts and displacement timeseries using wavelet decomposition. *Bull. Earthq. Eng.* **2010**, *8*, 231–255. [CrossRef]
9. Kamai, R.; Abrahamson, N. Are Near-Fault Fling Effects Captured in the New NGA West2 Ground Motion Models? *Earthq. Spectra* **2015**, *31*, 1629–1645. [CrossRef]
10. Boore, D.M.; Akkar, S. Effect of causal and acausal filters on elastic and inelastic response spectra. *Earthq. Eng. Struct. Dyn.* **2003**, *32*, 1729–1748. [CrossRef]
11. Pal, S.; Dasaka, S.S.; Jain, A.K. Inelastic response spectra. *Comput. Struct.* **1987**, *25*, 335–344. [CrossRef]
12. Tena-Colunga, A. Displacement ductility demand spectra for the seismic evaluation of structures. *Eng. Struct.* **2001**, *23*, 1319–1330. [CrossRef]

13. Mahin, S.A.; Lin, J. *Construction of Inelastic Response Spectra for Single-Degree-of-Freedom Systems*; (UCB/EERC-83/17); Earthquake Engineering Center, University of California: Berkeley, CA, USA, 1983.

14. Musson, R.M.W. Effective Peak Acceleration as a Parameter for Seismic Hazard Studies. In Proceedings of the 12th European Conference on Earthquake Engineering, London, UK, 9–13 September 2002.

15. Newmark, N.M.; Hall, W.J. *Earthquake Spectra and Design*; Earthquake Engineering Research Institute: Los Angeles, CA, USA, 1982.

16. Matheu, E.E.; Yule, D.E.; Kala, R.V. *Determination of Standard Response Spectra and Effective Peak Ground Accelerations for Seismic Design and Evaluation*; (ERDC/CHL CHETN-VI-41); U.S. Army Engineer Research and Development Center: Vicksburg, MS, USA, 2005.

17. Vamvatsikos, D.; Cornell, C.A. Incremental dynamic analysis. *Earthq. Eng. Struct. Dyn.* **2002**, *31*, 491–514. [CrossRef]

18. Somerville, P.G.; Smith, N.F.; Graves, R.W.; Abrahamson, N.A. Modification of Empirical Strong Ground Motion Attenuation Relations to Include the Amplitude and Duration Effects of Rupture Directivity. *Seismol. Res. Lett.* **1997**, *68*, 199–222. [CrossRef]

19. Champion, C.; Liel, A. The effect of near-fault adirectivity on building seismic collapse risk. *Earthq. Eng. Struct. Dyn.* **2012**, *41*, 1391–1409. [CrossRef]

20. Baker, J.W. Quantitative classification of near-fault ground motions using wavelet analysis. *Bull. Seismol. Soc. Am.* **2007**, *97*, 1486–1501. [CrossRef]

21. Soroushian, A. A technique for time integration analysis with steps larger than the excitation steps. *Commun. Numer. Methods Eng.* **2008**, *24*, 2087–2111. [CrossRef]

22. Nigam, N.C.; Jennings, P.C. Calculation of response spectra from strong-motion earthquake records. *Bull. Seismol. Soc. Am.* **1969**, *59*, 909–922. [CrossRef]

23. Boore, D.M.; Goulet, C.A. The effect of sampling rate and anti-aliasing filters on high-frequency response spectra. *Bull. Earthq. Eng.* **2014**, *12*, 203–216. [CrossRef]

24. Proakis, J.G.; Manolakis, D. *Digital Signal Processing: Principles, Algorithms and Applications*, 4th ed.; Pearson: London, UK, 2006; ISBN 978-0131873742.

25. Graizer, V. Effect of Low-Pass Filtering and Re-Sampling on Spectral and Peak Ground Acceleration in Strong-Motion Records. In Proceedings of the 15th World Conference of Earthquake Engineering, Lisbon, Portugal, 24–28 September 2012; pp. 24–28.

26. Douglas, J.; Boore, D.M. High-frequency filtering of strong-motion records. *Bull. Earthq. Eng.* **2011**, *9*, 395–409. [CrossRef]

27. Kanade, V.V.; Dawari, B.M. Prediction of Plastic motion under strong earthquakes using Rigid-plastic Response. In Proceedings of the 2015 International Conference on Industrial Instrumentation and Control (ICIC), Pune, India, 28–30 May 2015; pp. 1665–1669. [CrossRef]

28. Paglietti, A.; Porcu, M.C. Rigid–plastic approximation to predict plastic motion under strong earthquakes. *Earthq. Eng. Struct. Dyn.* **2001**, *30*, 115–126. [CrossRef]

29. Garini, E.; Gazetas, G. Rocking and Sliding Potential of the 2014 Cephalonia, Greece Earthquakes. In Proceedings of the 1st International Conference on Natural Hazards & Infrastructure (ICONHIC 2016), Chania, Greece, 28–30 June 2016.

30. Gazetas, G. Should Elastic Response Spectra be the Basis of Seismic Design of Strongly Inelastic and Soft-Soil–Structure Systems? In Proceedings of the 3rd International Symposium on Advances in Urban Safety, Nanjing, China, 24–25 November 2012.

31. Fan, C.L.; Zhang, S.Y. Rigid-plastic seismic design of reinforced concrete shear wall. *Int. J. Mod. Phys. B* **2008**, *22*, 5740–5746. [CrossRef]

32. Porcu, M.C.; Mascia, M. Rigid-Plastic Pseudo-Spectra: Peak Response Charts for Seismic Design. *Eur. Earthq. Eng.* **2006**, *3*, 37–47.

33. Chopra, A.K. Dynamics of Structures. In *Theory and Applications to Earthquake Engineering*, 5th ed.; Pearson: London, UK, 2016; ISBN 978-013455512.

34. Paultre, P. Response to Earthquake Excitation. In *Dynamics of Structures*; Wiley: Hoboken, NJ, USA, 2013; pp. 307–345. [CrossRef]

35. Tena-Colunga, A. Simplified seismic evaluation of existing structures. In Proceedings of the 8th Canadian Conference on Earthquake Engineering, Vancouver, BC, Canada, 13–16 June 1999; pp. 317–322.

36. Mashayekhi, M.; Harati, M.; Darzi, A.; Estekanchi, H.E. Incorporation of strong motion duration in incremental-based seismic assessments. *Eng. Struct.* **2020**, *223*, 111144. [CrossRef]

37. Deng, P.; Pei, S.; van de Lindt, J.W.; Liu, H.; Zhang, C. An approach to quantify the influence of ground motion uncertainty on elastoplastic system acceleration in incremental dynamic analysis. *Adv. Struct. Eng.* **2017**, *20*, 1744–1756. [CrossRef]

38. Krawinkler, H.; Parisi, F.; Ibarra, L.; Ayoub, A.; Medina, R. *Development of a Testing Protocol for Woodframe Structures*; (CUREE publication No. W-02); Consortium of Universities for Research in Earthquake Engineering (CUREE): Richmond, CA, USA, 2001.

39. De Luca, F.; Vamvatsikos, D.; Iervolino, I. Near-optimal bilinear fit of capacity curves for equivalent SDOF analysis. In Proceedings of the 3rd ECCOMAS Thematic Conference on Computational Methods in Structural Dynamics and Earthquake Engineering (COMPDYN 2011), Corfu, Greece, 26–28 May 2011; pp. 2470–2486.

40. Shahi, S.K.; Baker, J.W. An Efficient Algorithm to Identify Strong—Velocity Pulses in Multicomponent Ground Motions. *Bull. Seismol. Soc. Am.* **2014**, *104*, 2456–2466. [CrossRef]

41. Zhou, X.; Tamma, K.K. Design, analysis, and synthesis of generalized single step single solve and optimal algorithms for structural dynamics. *Int. J. Numer. Methods Eng.* **2004**, *59*, 597–668. [CrossRef]

42. Papazafeiropoulos, G.; Plevris, V.; Papadrakakis, M. A generalized algorithm framework for non-linear structural dynamics. *Bull. Earthq. Eng.* **2017**, *15*, 411–441. [CrossRef]

43. Lagaros, N.D.; Plevris, V. Artificial Intelligence (AI) Applied in Civil Engineering. *Appl. Sci.* **2022**, *12*, 7595. [CrossRef]

44. Lagaros, N.D.; Plevris, V. (Eds.) . *Artificial Intelligence (AI) Applied in Civil Engineering*; MDPI: Basel, Switzerland, 2022; p. 698. [CrossRef]
45. Plevris, V.; Ahmad, A.; Lagaros, N.D. (Eds.) . *Artificial Intelligence and Machine Learning Techniques for Civil Engineering*; IGI Global: Hershey, PA, USA, 2023. [CrossRef]